water

MDPI

Article

Assessing Seagrass Restoration Actions through a Micro-Bathymetry Survey Approach (Italy, Mediterranean Sea)

Sante Francesco Rende [1,*], Alessandro Bosman [1,2], Fabio Menna [3], Antonio Lagudi [4], Fabio Bruno [4], Umberto Severino [4], Monica Montefalcone [5], Andrew D. Irving [6], Vincenzo Raimondi [7], Sebastiano Calvo [7,8], Gerard Pergent [9], Christine Pergent-Martinì [9] and Agostino Tomasello [8]

1 ISPRA, Italian National Institute for Environmental Protection and Research, Via Vitaliano Brancati 60, 00144 Rome, Italy; alessandro.bosman@cnr.it
2 Istituto di Geologia Ambientale e Geoingegneria, Consiglio Nazionale delle Ricerche (CNR-IGAG), Via Eudossiana 18, 00184 Rome, Italy
3 3DOM—3D Optical Metrology Unit, FBK—Bruno Kessler Foundation, 38123 Trento, Italy; fmenna@fbk.eu
4 Department of Mechanical, Energy and Management Engineering DIMEG, University of Calabria, 87036 Arcavacata di Rende, Italy; antonio.lagudi@unical.it (A.L.); fabio.bruno@unical.it (F.B.); umberto.severino@unical.it (U.S.)
5 Department of Earth, Environment and Life Science, University of Genoa, 16132 Genoa, Italy; monica.montefalcone@unige.it
6 Coastal Marine Ecosystems Research Centre (CMERC), CQUniversity, Gladstone, QLD 4701, Australia; a.irving@cqu.edu.au
7 Biosurvey S.r.l., Academic Spin-Off University of Palermo, c/o ARCA, VialedelleScienze Ed. 16, 90128 Palermo, Italy; raimondi_vincenzo@yahoo.it (V.R.); sebastiano.calvo@unipa.it (S.C.)
8 Department of Earth and Marine Science (DiSTeM), University of Palermo, Viale delle Scienze Ed. 16, 90128 Palermo, Italy; agostino.tomasello@unipa.it
9 Coastal Ecosystem Team, University of Corsica, UMR 6134, BP 52, 20250 Corte, France; pergent@univ-corse.fr (G.P.); pmartini@univ-corse.fr (C.P.-M.)
* Correspondence: francesco.rende@isprambiente.it

Abstract: Underwater photogrammetry provides a means of generating high-resolution products such as dense point clouds, 3D models, and orthomosaics with centimetric scale resolutions. Underwater photogrammetric models can be used to monitor the growth and expansion of benthic communities, including the assessment of the conservation status of seagrass beds and their change over time (time lapse micro-bathymetry) with OBIA classifications (Object-Based Image Analysis). However, one of the most complex aspects of underwater photogrammetry is the accuracy of the 3D models for both the horizontal and vertical components used to estimate the surfaces and volumes of biomass. In this study, a photogrammetry-based micro-bathymetry approach was applied to monitor *Posidonia oceanica* restoration actions. A procedure for rectifying both the horizontal and vertical elevation data was developed using soundings from high-resolution multibeam bathymetry. Furthermore, a 3D trilateration technique was also tested to collect Ground Control Points (GCPs) together with reference scale bars, both used to estimate the accuracy of the models and orthomosaics. The root mean square error (RMSE) value obtained for the horizontal planimetric measurements was 0.05 m, while the RMSE value for the depth was 0.11 m. Underwater photogrammetry, if properly applied, can provide very high-resolution and accurate models for monitoring seagrass restoration actions for ecological recovery and can be useful for other research purposes in geological and environmental monitoring.

Keywords: *Posidonia oceanica*; habitat restoration; bathymetry; Structure from Motion; underwater photogrammetry; multibeam; monitoring

Citation: Rende, S.F.; Bosman, A.; Menna, F.; Lagudi, A.; Bruno, F.; Severino, U.; Montefalcone, M.; Irving, A.D.; Raimondi, V.; Calvo, S.; et al. Assessing Seagrass Restoration Actions through a Micro-Bathymetry Survey Approach (Italy, Mediterranean Sea). *Water* **2022**, *14*, 1285. https://doi.org/10.3390/w14081285

Academic Editor: Changming Dong

Received: 26 August 2021
Accepted: 11 April 2022
Published: 15 April 2022

1. Introduction

1.1. Seagrass Mapping

Seagrasses play a key ecological and economic role in coastal ecosystems worldwide, being important primary producers, performing functions of filtering coastal waters, dissipating wave energy to prevent the erosion of sandy shores, stabilizing and structuring the seabed, providing habitat and nursery areas for many organisms, and playing a major role in the mitigation of climate change through carbon sequestration [1–3].

Despite their importance, they are globally declining at an alarming rate [4], mainly due to poor coastal water quality and coastal development [5]. Currently, active seagrass restoration is considered a necessary strategy to counteract the loss of seagrass meadows and associated ecosystem services in addition to the efforts to conserve existing meadows and reduce human pressure on marine ecosystems [6,7].

The restoration of seagrass is a practice that has been adopted for several species around the world and began about 70 years ago [8]. Seagrass restoration interventions are conducted to compensate for habitat loss due to the construction of coastal structures or to restore ecosystem functionality in habitats that have undergone strong anthropogenic impacts, such as anchorages and mooring fields associated with recreational activities and boats and the effects of trawling.

Recently, there has been an increase in studies aimed at restoring degraded marine environments which has led to a proliferation of strategies and methodologies to enhance the effectiveness of restoration plans. However, there exists very high variability in outcomes, depending on the species, the methodologies employed, and the different environmental conditions encountered, such that the issue of seagrass restoration is still vigorously debated and a fully shared and standardized approach is far from being achieved [7,8].

Several descriptors collected at different levels of ecological complexity are gener-ally needed to assess seagrass restoration outcomes, from individuals (e.g., leaf biometry) to seascapes (e.g., spatial extent of restored area) [6]. Data concerning the spatial distribution of restored seagrass are of crucial importance for assessing its effectiveness, since the lack of accurate information concerning the extent of restored seafloor and the exact position of boundaries prevents any possible full evaluation of restoration success. Therefore, it is fundamental to be able to precisely identify and locate in space (geolocate) the boundaries of the initial restoration areas and to follow them through time in order to determine exactly how they change in space in the short, medium, and long term.

Different techniques for seagrass mapping have been refined over the years based on active high-resolution geophysical data and remote sensing, i.e., Multibeam Echo-Sounding (MBES), Side Scan Sonar (SSS), and Laser Imaging Detection and Ranging (LIDAR), [9–14] or on passive panchromatic and multi-spectral data, i.e., Unmanned Aerial Vehicle (UAV) and satellite imagery [15–17].

The MBES survey allows for the acquisition of higher resolution (from 0.3 m to 0.05 m resolution) bathymetry and backscatter data in shallow water (1 m to 300 m) [14] and provides a 3D reconstruction of the seafloor and a map of acoustic response, respectively. The Multispectral Satellite Image (MSI) technique provides data with spatial resolutions between approximately 2 m and 0.5 m. However, these geophysical and multispectral techniques do not have sufficient resolution to define in detail the spatial location and the number of restored plants. Recently, photogrammetry, widely used for terrestrial applications, has also been used as a detailed and accurate underwater survey tool for monitoring marine benthic habitats. Previous works have shown that photogrammetric products can provide ultra-high-resolution (from about 0.02 m to 0.001 m resolution scale) orthomosaics/Digital Elevation Models (DEMs) characterized by high precision [10,14,18–21]. Recent advances in photogrammetry using Structure from Motion (SfM) and multi-view stereo (MVS) algorithms have led to the proliferation of 3D digital representations (i.e., Dense Point Clouds (DPCs)) and DEMs of marine habitats, from which structural complexity can be estimated [18]. These techniques have become very popular during the last decade and are now extensively used in marine ecology to study the interactions

between habitat structure and ecological assemblages [22–25]. The application of underwater photogrammetry to seagrass mapping has recently become more accessible owing to the availability of different software packages [26,27] that improve automation and ease of use. A very complex seagrass restoration monitoring protocol involves a small boat equipped with GNSS–RTK and a digital depth sensor and a diver operator with an underwater propulsion vehicle to perform the photogrammetric survey [28]. Nevertheless, to guarantee reliable photogrammetric products of centimetric resolution, several factors and procedures need to be adopted, from camera calibration [29,30] to the use of reference targets and image enhancement techniques [31], which together represent critical aspects to be considered for obtaining 3D models and ultra-high-resolution orthomosaics of proven quality [19].

Underwater photogrammetric surveys can be performed with an autonomous surface vehicle (ASV) [14] (Figure 1a), an autonomous underwater vehicle (AUV) equipped with HD cameras and an inertial navigation system [32–34], by scuba diving (Figure 1b), with underwater towed video camera systems (UTCS) [15] (Figure 1c), and, finally, by using a remote operated vehicle (ROV) equipped with cameras and acoustic transducers [35] (Figure 1d).

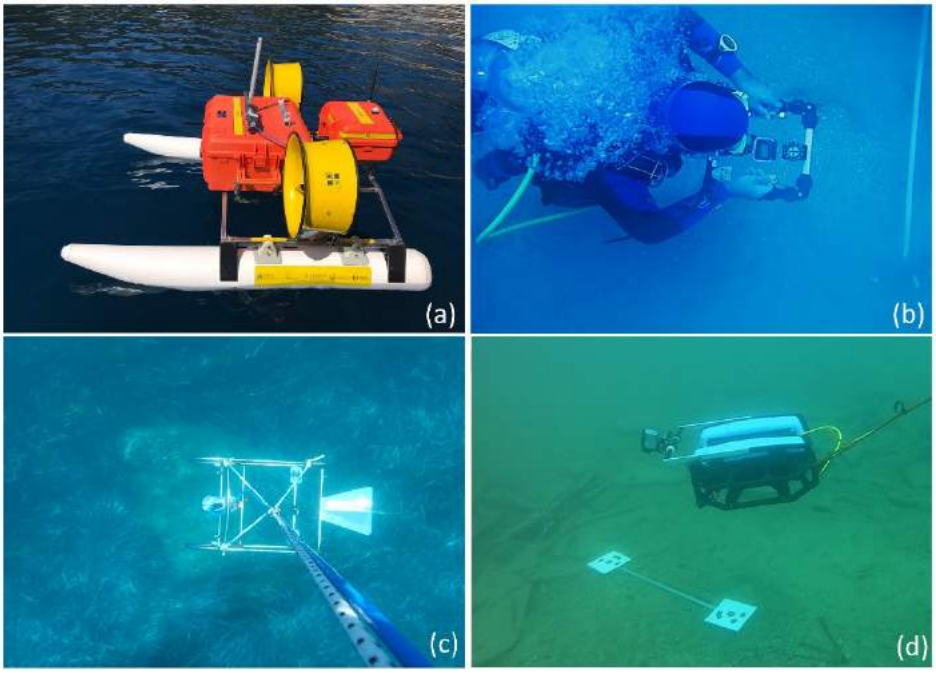

Figure 1. Examples of the photogrammetric multisensory platforms: (**a**) an autonomous surface vehicle (ASV), also called a development vehicle for scientific survey (DEVSS); (**b**) scuba diving; (**c**) underwater towed video camera systems (UTCS); and (**d**) remote operated vehicle (ROV).

Although most of the photogrammetric products are still obtained in post-processing, after the survey, the current trend is to provide 3D measurements in real time using visual Simultaneous Localization and Mapping (vSLAM) techniques such as the ORUS 3D System by COMEX [36] and SubSLAM X2 from VAARST https://vaarst.com/subslam-3d-imaging-technology/ (accessed on 10 March 2022).

1.2. Georeferencing and Scaling Techniques

The georeferencing of photogrammetric surveys is one of the most complex procedures to implement underwater [19,37–42] but is of utmost importance for different kinds of scientific analyses. The photogrammetric process requires at least one known reference distance to provide metric results. However, as in all surveying disciplines, redundancy is sought to provide reliable results, thus requiring more than a single distance measurement

(for example, when applying the trilateration technique to well distributed 3D GCPs—see Section 2.8). This reference distance can be measured directly from the object to be surveyed, inferred from surveyed 3D coordinates using geodetic techniques (GNSS) [38,43], or be implicitly part of the sensor calibration procedure. Indeed, metric measurements can be obtained using synchronized stereo and multi-camera systems. These have been a popular solution for several years in different application fields [44–46], demonstrating great flexibility and the ability to measure even dynamic scenes, such as moving fish for aquaculture applications [46]. However, these benefits often come at an increased cost of multiple sensors, more power, and a heavier and more cumbersome capturing system [36]. To provide scaled photogrammetric measurements, laser pointers have been a popular low-cost solution for single camera systems [47–49]: they require the relative orientation of the laser direction with respect to the camera and custom algorithms to detect the laser spot in the image to perform forward triangulation. Recently, a novel approach for scaling and levelling to the local vertical direction in an underwater photogrammetric survey was presented in [49]. The method integrates depth measurements from a high-resolution pressure sensor providing an accuracy potential better than 1:5000 for the length measurement and 0.025 degrees in the horizontal levelling.

Depending on the type of technology used and the requirements of the application, the accuracy of the available surveying techniques might not be sufficient, with an overall increased complexity of surveys when these are conducted at greater depths [32,37].

An alternative method to GNSS Real-Time Kinematics or Post-Processing Kinematics surveys in very shallow waters to collect control points is to use the 3D trilateration technique which is very common in maritime archaeology and is known as the Direct Survey Method [50]. The 3D Trilateration procedure is used for obtaining metrically correct products, such as dense point clouds, DEMs, and orthophotos, and is based on a network of ground control points (GCPs) whose linear distance and depth measurements must be known [38]. A typical implementation underwater is carried out by measuring distances with a tape and taking depth measurements with a dive computer [51–53]. An improved technique that can achieve sub-centimetric accuracy via underwater photogrammetry was recently demonstrated in the context of long-term monitoring of coral growth in French Polynesia [19,52]. The technique implements underwater control networks that combine 3D trilateration and geometric levelling to overcome the limitations imposed by the poor accuracy of depth measurements taken with dive computers [53].

For deep surveys, an ultra-short baseline acoustic positioning system (USBL) and support vessels must track the carrier system (i.e., ROV, AUV), while, for very shallow surveys, direct photogrammetry [54] with an image acquisition platform that integrates a global navigation satellite system (GNSS) is required [55]. Effective results can be obtained by coupling a method for georeferencing underwater photogrammetric mapping performed by scuba diving with high resolution MBES data [55]. A procedure, tested in this work, involves a co-registration between different optical and acoustic datasets through the identification of homologous points between two datasets. This procedure is performed manually through a rectification process that allows the georeferencing, scaling, and aligning of the DEM with the LAS data (latter represents the file format for the interchange of 3D point cloud data) with the DEM. Data rectification is perfomed using ground control points (GCPs) that can be manually entered or chosen from the reference data. A technique to automate the co-registration of high-resolution image blocks and multibeam acoustic data involves the use of permanent optoacoustic markers [56].

1.3. Image and Point Cloud Classification

Object-Based Image Analysis (OBIA) is an advanced classification method that incorporates spectral data, weight, color, texture, shape, and contextual information to identify thematic classes in optical and acoustic data-derived images [57]. The OBIA classification uses a multiresolution segmentation of the image to identify homogeneous objects

(note: the term "object" in this case stands for a contiguous group of spatial data, such as pixels in a bathymetric grid).

The segmentation process is based on predefined parameters, such as compactness, shape and scale, derived from real-world knowledge of the characteristics to be identified and classified. For machine learning-based mapping, several algorithms such as Support Vector Machine (SVM), Random Tree (RT), Decision Tree (DT), Bayesian, and k-Nearest Neighbor (k-NN) algorithms have been further refined, are accessible with various data analysis software, and have been developed to improve either classification or seagrass prediction from satellite imagery and UAV orthomosaics [58].

Point cloud analysis is commonly performed to classify terrestrial LIDAR data. Both point clouds obtained by LAS LIDAR and by photogrammetry can be easily classified using specific software. A recent review study by Bedenko et al. [59] compares different classification software applications.

Further advantages derived from the combination of both methods have been recently implemented, improving the quality of the results in terms of the accuracy and resolution of seagrass identification and positioning [13,14].

However, in the context of the seagrass restoration process, remote sensing methods have been used exclusively for restoration plans, especially for habitat mapping to support site selection [60–62]. In contrast, the application of such methodologies in a post-restoration phase to assess restoration performance is still very limited. For example, a simple underwater photomosaic of a small transplantation with *Posidonia oceanica* was acquired for the first time using optical data, which also allowed the assessment of the coverage achieved by the transplanted seagrasses 12 years after the initial intervention [63]. Although a photomosaic of the entire transplant seen from above was obtained, the pictures were not accompanied by cartographic accuracy values. Therefore, the errors associated with the use of these methods in mapping seagrass restoration remain to be assessed. This work aims at defining an operational, very high-resolution, cost-effective methodology based on a multi-image photogrammetric approach to achieve effective assessment of medium- to long-term seagrass transplantation performance. In this paper, we mainly present the results of experiments carried out at two sites in the Mediterranean Sea.

2. Materials and Methods

2.1. Study Sites

Photogrammetric surveys were conducted on *Posidonia oceanica* sites located in five different areas, four of which are in Italy (the central and southern Tyrrhenian Sea and the Strait of Sicily) and one in France (the central Tyrrhenian Sea). All the areas presented here fall within Italian and French areas of biological interest as marine protected areas (MPAs) and special areas of conservation (SACs).

Three sites include restored *P. oceanica* meadows: Sant'Amanza, Infreschi Bay, and Capo Feto (Figure 2), while two sites (Cirella and Ventotene Island, Figure 2) have been studied because monitoring will be carried out in the future. All restoration activities were performed using a *P. oceanica* anchoring support-patented product (n. 0001400800/2010 and n. 102015000081824/2018), made of totally biodegradable polymer (Mater-Bi®, Novara, Italy) [7].

Around Cirella Island (Calabria region 39.697727° N, 15.804926° E) an underwater photogrammetry survey was carried out in July 2019 at a water depth between 4 m and 14.5 m (Figure 2) and in June 2021 at Ventotene Island (40.803825° N, 13.431503° E) at a water depth of 13.8 m. In October 2020, an underwater photogrammetry survey of *P. oceanica* restoration was conducted at Capo Feto (37.655856° N, 12.536330° E) located in the south-western sector of Sicily (Figure 2) by scuba divers at a 6.5 m depth. In March 2021, a photogrammetric survey was conducted at the restored site of Infreschi Bay (39.998177° N, 15.425601° E), located in the Campania region, at a 4 m water depth. Finally, surveys were performed in June 2021, in the south-western part of Corsica Island (France), at the restored site of Sant'Amanza (41.431499° N, 9.230639° E), at a 14.5 m water depth (Figure 2).

Figure 2. Location of the three restored (yellow) and two tests sites (red) conducted in France in the central Tyrrhenian Sea (Corsica) and in Italy in the central and southern Tyrrhenian Sea (Ventotene, Cirella Islands, and Infreschi Bay) and in the Sicily Channel (Capo Feto). The Italian areas are located in marine protected areas (MPAs) and in special areas of conservation (SACs).

2.2. Equipment, Camera Calibration, and Survey Techniques

For the activities carried out at the study sites, we have summarized the workflow (Figure 3) adopted for underwater photogrammetric surveys and data analysis (Figure 3) which was composed of four steps (i.e., pre-survey, survey, processing, and data analysis). In particular, we defined underwater photogrammetric activities according to the following eight phases: Phase 1 involves the planning of the image acquisition path; Phase 2 involves the on-site camera calibration; Phase 3 involves the installation of the reference markers on the seafloor; Phase 4 involves setting the relative height of the camera from the sea bottom and data acquisition; Phase 5 involves the image enhancement of the data via post-processing; Phase 6 involves the processing chain of the frames using photogrammetry software; Phase 7 involves the classification using machine learning and object image analysis (OBIA) of the seafloor morphologies and features; Phase 8 involves the dense point cloud analysis, measurements, and time-lapse analysis (Figure 3).

2.3. Camera Pre-Calibration

Camera calibration is the process of determining camera interior orientation parameters, namely, focal length, principal point coordinates, and radial and decentring lens distortions [64]. Most cameras are not designed to work directly underwater, and a waterproof housing is necessary. Depending on the type of port used by the housing, different refractive phenomena are introduced [65,66] that need to be taken into account with proper mathematical modeling and underwater calibration. Camera calibration parameters can be recovered in self-calibration as part of the photogrammetric process if proper acquisition protocols are followed [67]. Further details on underwater calibration methods and techniques can be found in [68].

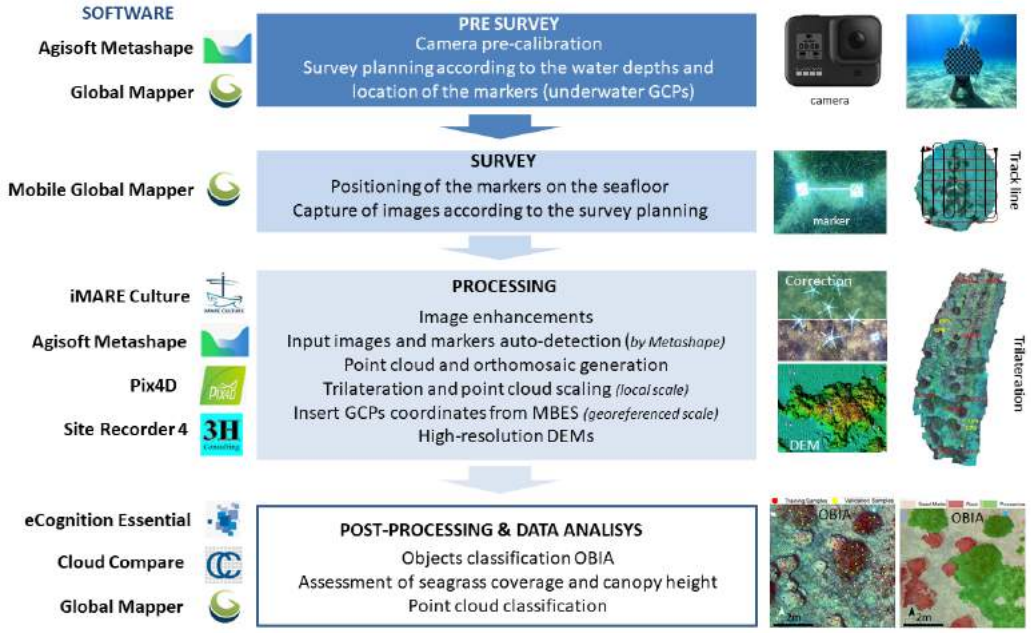

Figure 3. Workflow used for the underwater photogrammetric survey and data analysis for very high-resolution mapping of *Posidonia oceanica* site restorations. The activities include pre-survey, survey, processing and analysis, post-processing, classification of the seafloor, and time-lapse analysis.

When dealing with more expeditive survey acquisitions or if the seabed is largely covered by species that are not static during the photogrammetric survey, such as the Posidonia under current and swell, it is advisable to perform a dedicated underwater camera calibration using a portable test field before the actual survey. Indeed, the assumption made in photogrammetry that tie points lie on an object's surface, considered as a rigid body, is often invalidated by the moving leaves, possibly introducing significant matching errors and outliers in the orientation and self-calibration process.

For our projects, the GoPro Hero 4 black edition action camera was used for image acquisition during field surveys (Figure 4a). GoPro action cameras are well known to the scientific community and are extensively used for different underwater photogrammetry projects [69–71]. The camera features a 12 MPs (4000 × 3000 pixel) 1/2.3″ sensor (6.17 mm × 4.55 mm) with a pixel size of 1.5 µm and is equipped with a fisheye lens with fixed focus whose nominal focal length is 2.9 mm. The camera is sold with an acrylic waterproof housing that features a flat port.

The camera was calibrated using a medium format field of view, which utilizes a reduced part of the sensor by cropping the original image to 3000 × 2250 pixels. Image acquisition was carried out underwater using a rigid planar chessboard pattern (Figures 4b and 5) according to the procedure adopted in previous studies [22]. Multiple images of the pattern were taken by framing the chessboard with different orientations at the operative depth and at a distance between 1 and 2 m, right before the photogrammetric survey (Figure 5). The calibration was processed using a tool available in the Agisoft Metashape Pro 1.7.2 version software [72].

The calibration provided values of the interior orientation parameters, used to determine the FOV of the GoPro Hero 4 cameras in water. Afterwards, using these parameters, FOV and GSD (Ground Sample Distance) of the GoPro 4 camera were determined using an Excel spreadsheet and utilized for the planning of the image acquisition path.

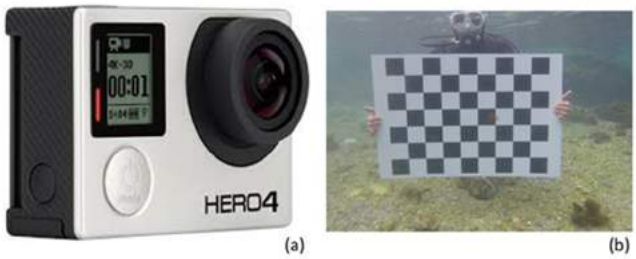

Figure 4. (**a**) GoPro HERO 4 Black camera used for seafloor mapping. (**b**) Example of underwater image of the chessboard used used for camera calibration.

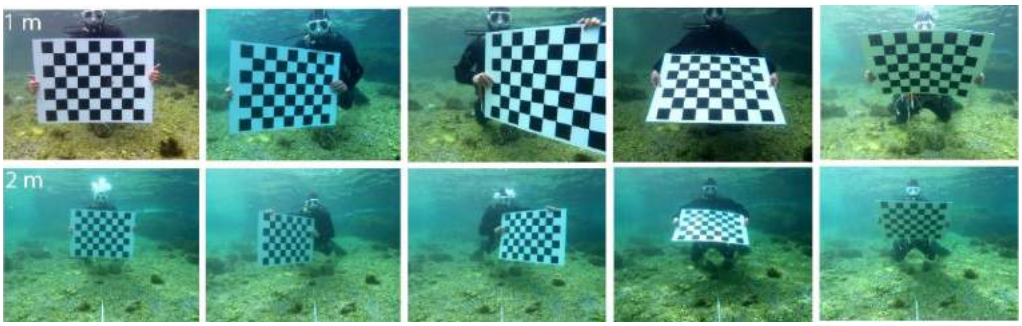

Figure 5. An example of GoPro 4 Black camera calibration on site using the chessboard at different angles and distances.

2.4. Underwater Photogrammetric Survey

For each survey, the diver acquired images at a maximum distance of 3.5–4 m above the sea floor, following straight paths along parallel and regularly spaced strips. Furthermore, according to standard photogrammetry protocols, the diver also performed across-track strips (Figure 6). A swimming speed of about 5–20 m min^{-1} was maintained during the survey and the images were acquired in timelapse mode with a time interval of 0.5 s. The planned path made of parallel and cross strips was followed by the diver with the help of an underwater compass. The length of the transects and the distance of successive lines were programmed on the basis of the known FOV of the camera. Targeted GCPs, placed on the bottom, supported the diver's navigation in course inversions. The high overlap and sidelap percentages chosen for the photogrammetric survey make sure that the site of interest is fully covered by the captured images.

All surveys were conducted by a scuba diver equipped with a Mares dive computer (Quad Air model) and a GoPro Hero 4 action camera Black edition set with a medium Field of View (FOV) to consider only the central part of the image, less affected by chromatic aberrations and astigmatism. As a result, the image resolution was 7 megapixels (Figure 4). The camera was pointed downward to obtain nadiral images with the diver swimming at the same height from the bottom.

The horizontal field of view (FOV) was calculated using the following formula [22]:

$$FOV = 2 \arctan [(w/2 \times f)]$$

where w is the width of the sensor and f is the calibrated focal length of the camera. The field of view in the height direction h of the sensor can be computed using h instead of w in the above formula. The coverage in object space along the width and height directions of the sensor, at different distances from the camera, was calculated (Table 1) using the following formula [22]:

$$Width = 2 \times d \times \tan (FOV/2)$$

This equation is very useful for planning 3D photogrammetric surveys in areas where seagrass is present and where depth and bottom areas are known variables. Knowing the

real FOV of the camera and the distance from the bottom, one can determine the effective bottom coverage of the images. Values for the width, height, area, and GSD of the image, as a function of the photographic shooting distance from the seafloor, have been calculated and are reported in Table 1. These values increase linearly with the distance from the bottom (Figure 7).

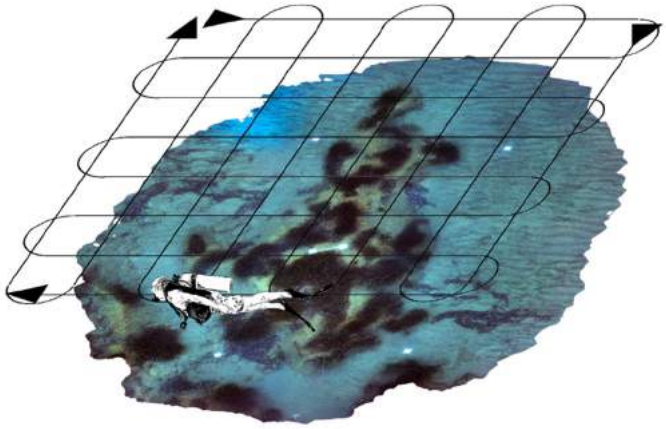

Figure 6. Navigation lines conducted by the diver at Ventotene Island during the photogrammetric survey in a time lapse with 0.5 s time interval at a water depth of about 3–4 m.

Table 1. Image with, height, surface, and Ground Sampling Distance (GSD) as a function of distance from the seafloor.

Distance (m)	Width (m)	Height (m)	Surface (m^2)	GSD cm
1	1.23	0.91	1.12	0.3
2	2.47	1.82	4.49	0.6
3	3.70	2.73	10.11	0.9
4	4.94	3.64	17.97	1.2
5	6.17	4.55	28.07	1.5
6	7.40	5.46	40.43	1.9
7	8.64	6.37	55.02	2.2

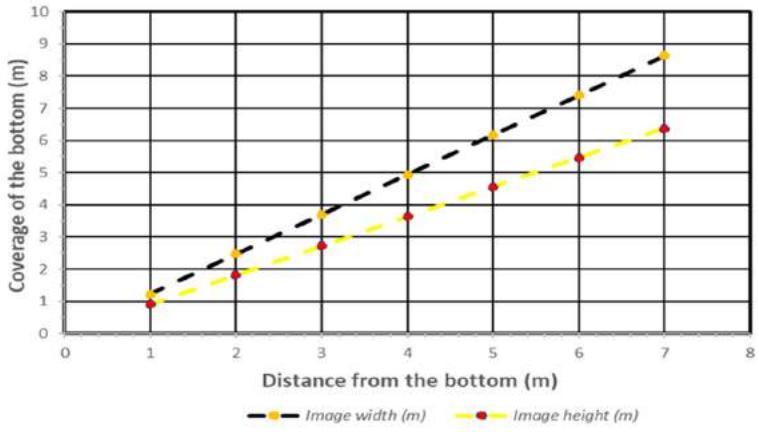

Figure 7. Image width and height as a function of the distance from the seafloor and the coverage of the bottom.

The calculated FOV value was 62.98°. The field widths of the frames were used for planning the path of the photogrammetric survey (the number of transects to be conducted and the height of the survey relative to the sea bottom) to guarantee the pre-planned overlap of 60–70% and a sidelap of 25–40% (Figures 6 and 7).

2.5. Multibeam Data Collection and Accuracy

At Capo Feto, a multibeam bathymetry survey was carried out in September 2019 before the photogrammetric survey. Data was collected with a Teledyne Reson SeaBat 7125 Echo-Sounder System at 400 kHz with a beam-width of 0.5° × 1° and a depth resolution of 5 mm, using a small boat.

Around Cirella Island, the multibeam survey was carried out in September 2018 before the photogrammetric survey. Data was collected at a water depth between 5 m and 40 m using a Kongsberg EM2040 at 400 kHz with a beam-width of 0.4° × 0.7° and a pulse length of 108 µs hull-mounted onboard of the R/V "Astrea", a 24 m-long boat.

Post-processed sounding multibeam data [14,73,74] were merged and gridded for the generation of DEMs at 0.1 m and 0.2 m cell size resolution, respectively.

The resolution and accuracy of bathymetric data collected depended on many factors: the depth of the survey (footprint size), the state of the sea (quality data), sensor frequency and wavelength of the signal used, GNSS positioning accuracy (Real-Time Kinematics, Post-Processing Kinematics), motion sensor quality, the type of installation of the multibeam sensor (pole or hull), ray-tracing correction on the soundings based on the sound speed velocity along the water column (vertical and horizontal) recorded through a velocity probe, as well as a local patch test to calibrate the multibeam sensor angles, local tide corrections for the vertical datum, statistical and manual deleting of the random and organized noise, and, finally, the generation of the weighted average grid for the depth range.

In shallow and very shallow waters we used high-frequency (400 kHz) sensors and performed the post-processing according to high hydrographic standards [14,73,74], obtaining centimetric vertical accuracy comparable to a kinematic laser scanner survey in Real-Time Kinematics mode. Backscatter intensity data for the seafloor and the water column [14] were recorded only for the survey conducted by Kongsberg EM2040 around Cirella Island.

2.6. Image Enhancement Tools

An underwater image enhancement technique was performed before the 3D reconstruction to minimize the effect of the water column on the underwater images [30]. Direct computation of ACE uses a polynomial approximation of the slope function to decompose the main computation into convolutions. The enhanced image appears natural because the input image is adjusted in a manner consistent with perception. Color correction was carried out using the image enhancement process tool (software developed by the iMARECULTURE Project) [75]. Specifically, we used the Automatic Color Enhancement (ACE) algorithm [76] (Figure 8). ACE is an effective method for color image enhancement based on modelling several low-level mechanisms of the human visual system.

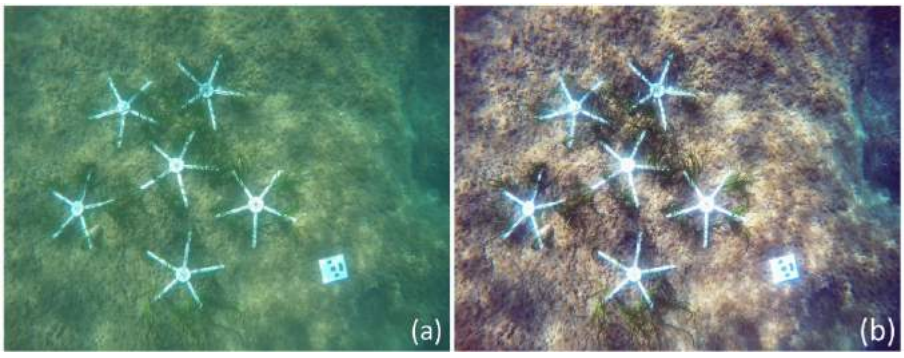

Figure 8. Comparison between before and after correction by the image enhancement algorithm (ACE) on a single frame of the underwater photogrammetric survey. The white stars indicate the restoration area of *P. oceanica*, while the white square at the bottom right indicates the circular coded targets for alignment of the frames. (**a**), image before (ACE) correction; (**b**), image after (ACE) correction.

2.7. Photogrammetric Processing

The photogrammetric processing was carried out using the commercial software Agisoft Metashape Pro V 1.7.2. The GCP position was identified using the automatic marker detection function. The image orientation was performed using the images at full resolution. The same resolution was used for the creation of the dense point cloud (exported in LAS format) and orthomosaic generation. For both the dense point cloud and the orthomosaic, accuracy was estimated using reference GCP targets and a known control scale bar (1 m).

2.8. Co-Registration of Multibeam Bathymetry and 3D Trilateration Data at Local Scale

Data co-registration between the dense point cloud LAS and DEMs from multibeam bathymetry data at Capo Feto was performed with the rectification tools of the Global Mapper software [77] using 12 Ground Control Points (GCPs) observable in the datasets. These GCPs are represented by very small morphological features and circular coded targets (Figure 9). The scale bars, visible in the LAS, were used as check measures to evaluate the geometric accuracy obtained after georeferencing the data.

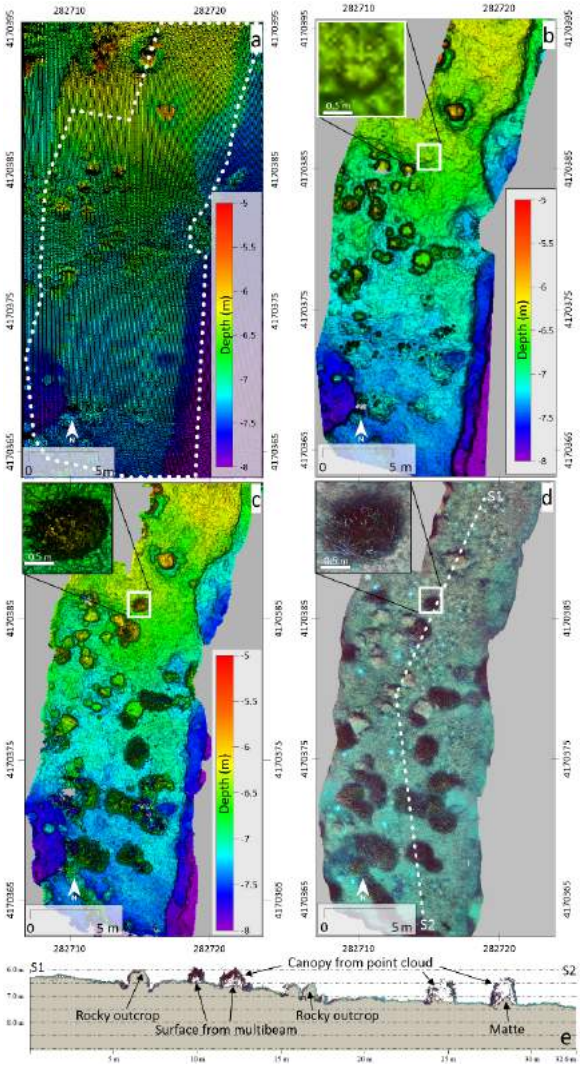

Figure 9. Overlapping soundings from multibeam data and dense point clouds. (**a**) Sounding map from multibeam data. (**b**) Digital Elevation Model at 0.05 m resolution from multibeam data. (**c**) DEM at 0.03 m from dense point cloud. (**d**) Orthomosaic at 0.01 m resolution. (**e**) The S1–S2 profile shows a comparison between the dense point cloud (canopy) and DEM from multibeam data. The white box indicates the same area of *P. oceanica* investigated with MBES and photogrammetry.

Georeferencing of the dense point cloud (X,Y,Z) extracted from photogrammetry was performed using the Global Mapper 22.1 LIDAR COMPARE tool [53]. Rectification or georeferencing is the process of assigning a geographic location, scale, and alignment to a file (known points). This is achieved using GCPs, which can be entered manually or chosen from loaded reference data. Although georeferencing is traditionally performed on raster data, the process can be applied to 3D vector data or point clouds as well. With point cloud, LIDAR data, DEMs, and mesh features, the rectification option displays a 3D layer control point dialog with options for adding 3D control points (X, Y, Z). This method of the 3D rectification used by Global Mapper software calculates a 3D affine transformation through a 4×4 matrix that best fits the control points.

This tool also supports the functionality of the "Compare Point Cloud LIDAR QC" tool and finds duplicate LIDAR points. This function identifies a point cloud that is different between 2 sets of point clouds and/or compares the elevations from loaded LIDAR point clouds to loaded 3D control points. It then adjusts the point cloud to match the GCP points through a triangulation algorithm.

Pairs of homologous points were identified between the georeferenced multibeam data (soundings) and point clouds obtained from photogrammetric restitution (not georeferenced). These points were used as GCPs. The procedure provides for the georeferencing of the scattered point cloud based on homologous points on the three components X, Y, and Z identified on both datasets. GCPs can be small objects, such as rocky outcrops and escarpments, and all morphological features that have well-defined geometric shapes.

The positions of the X, Y, and Z control points were inserted manually according to the correspondences of the objects and shapes present in the two datasets (Figure 9).

The 3D trilateration technique (known also as the Direct Survey Method (DSM) in underwater archaeological surveys) was applied to the survey sites. Specifically, a network of GCPs was realized for each site by using two reinforced quadrilaterals that were elaborated using Site Recorder 4 software [78] (see Figure 10). A control GCP network was realized at each survey site using circular coded targets from Agisoft Metashape. For each target, the relative depths and the six distances (four sides plus the two diagonals (GCP)) were measured by dive computers. Measurements of distances between GCPs and depths were taken in situ by divers. Metric scale bars of a known dimension of 1 m were used as control measures (Figure 10c). Finally, local coordinates were calculated using Site Recorder 4 software and associated with GCP markers with Agisoft Metashape software.

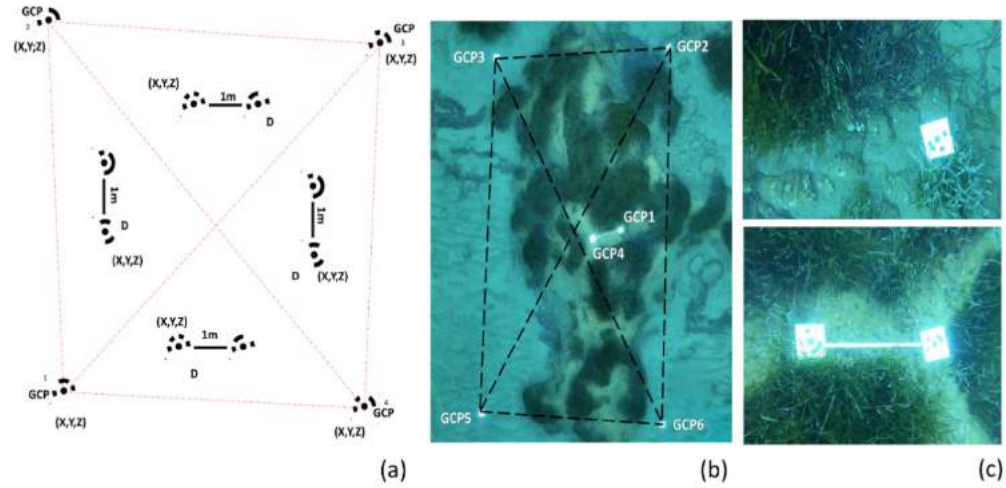

Figure 10. (**a**) Example of 3D trilateration of the reinforced quadrilateral control point network (GCP). (**b**) Example of marker positioning. (**c**) GCP and control bar.

2.9. Data Classification and Analysis

The Cape Feto orthomosaics were classified using an OBIA approach with the eCognition Essentials 1.3 software [79] and using a k-NN supervised classification algorithm.

The multiresolution segmentation algorithm was used to identify homogeneous objects. The process of multiresolution segmentation was carried out by considering the following parameters: scale factor, shape, smoothness, and compactness. We tested the performance of the k-NN supervised classification. The k-NN algorithm is a method for classifying objects by a majority ranking of their neighbours, with the object being assigned to the class most common among its k-nearest neighbours. The OBIA classification was performed using 163 ground-truth training samples. While of the classification accuracy was assessed using 76–98 ground-truth validation samples. Finally, user and producer accuracy and K-index were determined. The dense point cloud was classified with Global Mapper V 22.0 software using the LIDAR classification tool and the canopy height of the restoration site was analyzed and measured with Cloud Compare V 2.12 software [80].

3. Results

Processing of photogrammetric data of the Capo Feto site (Figure 2) allowed us to obtain a dense point cloud composed of about 20 million points and an orthomosaic with cells of 1 mm resolution (Figure 10a), while for the Sant'Amanza site the dense point cloud consisted of approximately 10 million points with an orthomosaic resolution of 1.4 mm (Figure 10b). Finally, for the Infreschi Bay site, the dense point cloud was composed of 12 million points and an orthomosaic resolution of 1 mm (Figure 11).

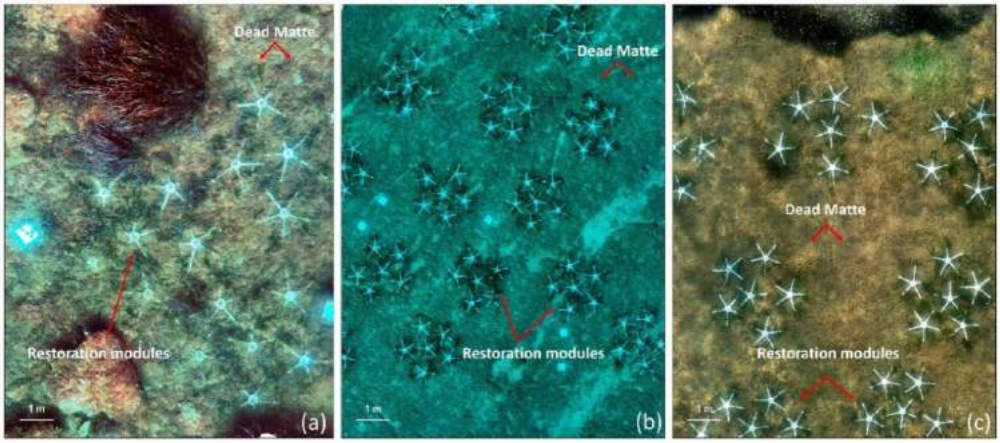

Figure 11. (**a**) Very high-resolution orthomosaics of the Capo Feto site (Sicily), (**b**) Sant'Amanza (Corsica Island), and (**c**) Infreschi Bay. White stars indicate the restoration area of *P. oceanica*.

The acoustic (MBES) and optical datasets of the Capo Feto site show perfectly matching morphological features (e.g., rocky outcrops), thus representing ideal candidate control points (GCPs) for the co-registration of the two datasets (Figure 12a,b). The corrected point cloud, using 12 GCPs identified between the two acoustic MBES and optical datasets, resulted in both the geo-referencing of the point cloud and the redefinition of the vertical elevation values of the optical LAS. Although the multibeam data from the Capo Feto site were not acquired at a very high resolution, we still obtained a discrete scaling (horizontal and vertical) of the optical LAS point cloud.

Although the density of sounding of the multibeam data was lower than the spatial resolution of the photogrammetric survey, the depth values of the bathymetric data had decimeter accuracy. In this regard, it should be noted that the footprint size of the Reson SeaBat 7125 multibeam sensor used was $0.5^\circ \times 0.1^\circ$. At 6 m depth, we obtained in the nadir sector an acoustic footprint with an area of 0.003 m^2 and one with an area of 0.01 m^2 in the outermost position at about 50°. On the other hand, the Kongsberg EM 2040 MBES features a footprint size of $0.4^\circ \times 0.7^\circ$ and this provides an even higher resolution. This characteristic is adequate in shallow and very shallow water for the georeferencing of point clouds generated by photogrammetry. Overall, the vertical RMSE was 0.06 and 0.05 for Cirella Island and Capo Feto, respectively.

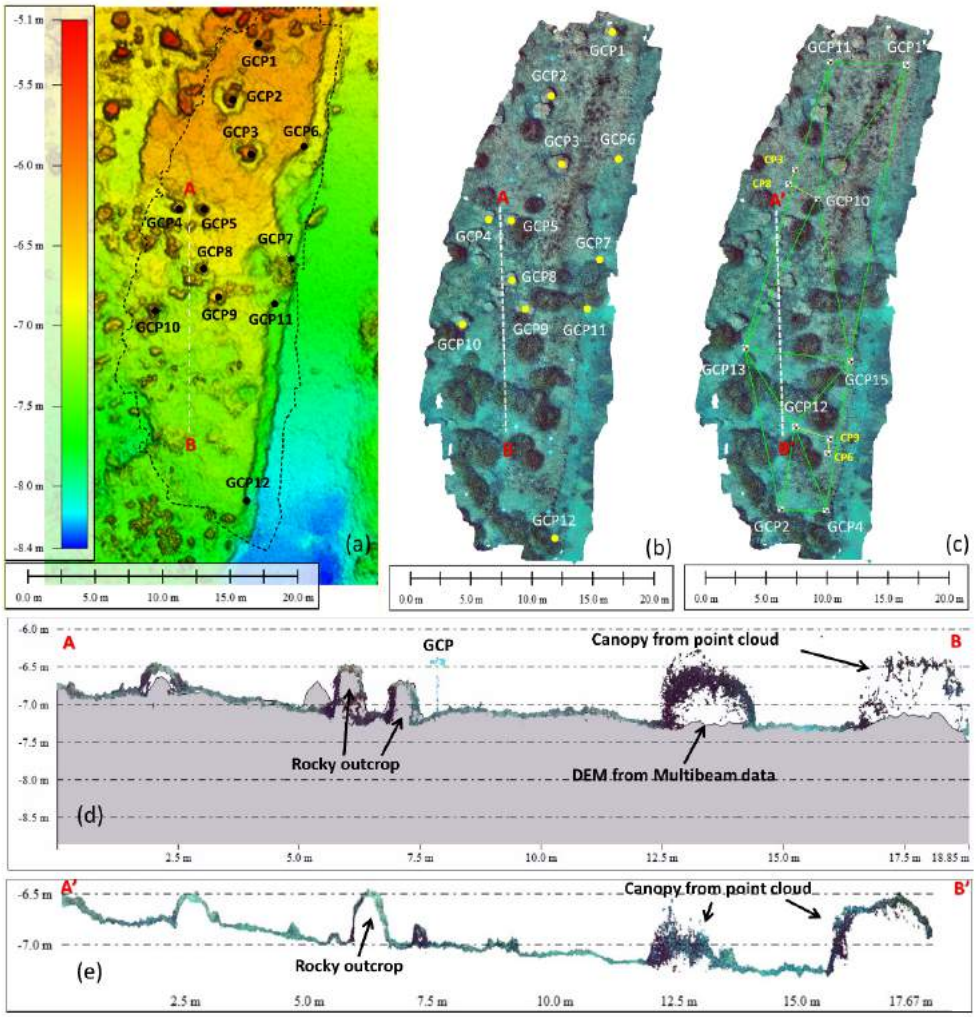

Figure 12. (**a**) DEM of Capo Feto at 5 cm of resolution, reconstructed from multibeam bathymetry. (**b**) Dense point cloud and location of control points (GCPs) used to georeferencethe the 3D model. (**c**) Three-dimensional trilateration technique: a closed grid consisting of eight ground control points (GCP) and two control bars, 1 metre in length, located on the seabed. (**d**) Bathymetric profile (MBES correction) along the transect (AB) shows the Canopy Height Model (CHM) Capo Feto (Sicily). (**e**) Bathymetric profile (trilateration correction) along the transect (A'B'). Capo Feto (Sicily).

This technique is very efficient and rapid, especially when used in large areas at shallow depths, where activities performed while SCUBA diving are safer with extended bottom time. However, this technique can also be applied at greater depths at which SCUBA dives may be more constrained by limited bottom time due to the no-decompression limit (NDL). As a disadvantage, the use of multibeam to georeference and scale the LAS point cloud has a high cost and is not always applicable in shallow water.

The scaling of the LAS point cloud performed using the 3D trilateration technique, using two reinforced squares composed of eight GCPs (Figure 12c), can be affected by limited accuracy of the depth measurement acquired by the underwater computers. This problem can be overcome using high-accuracy professional pressure sensors that are calibrated in situ with the local temperature, salinity, and density. However, GCP distance measurements acquired in situ by the dive operator may instead report errors related to the increased distance between GCPs. Unfortunately, distance measurements between GCPs performed in situ by divers greatly increase dive times, requiring first the arrangement of GCPs, then the acquisition of images with the camera, and finally the measurement of GCP depths and relative distances between them.

To speed up the scaling procedure over large areas, a good comprimise is to combine the use of known calibrated lengths (scale bars) with depth measurements from a dive computer. This procedure would considerably reduce the dive time since it would only be a matter of placing the targets on the bottom and measuring their depth. A further improvement of the execution times of the 3D trilateration surveys by divers could be obtained by using a pressure sensor coupled to the underwater camera during the survey of the images.

This technique is very effective, fast, and inexpensive if applied in small areas and at shallow depths at which scuba diving does not have time limits. As for disadvantages, the use of the 3D trilateration technique does not allow the georeferencing of the LAS point cloud since the spatial reference is given by local coordinates. Comparison of the AB transect vertical profiles of the dense point cloud corrected using multibeam data compared to the point cloud corrected using 3D trilateration show canopy height values between 0.5–1 m (Figure 12d,e). The point cloud, rectified with multibeam data, has more accurate planimetric and vertical Z-accuracy than the 3D trilateration.

From a statistical perspective, the 3D trilateration with eight points gave a total root mean square (RMS) residual of 0.007 m; the same value of the residuals RMS (0.003 m) was found for the planimetric and for the depth.

Table 2 shows the results of the planimetric distances between individual GCP markers taken between the two rectified datasets using the georeferencing technique and 3D trilateration. The root mean square error (RMSE) obtained for the planimetric measurements was 0.05 m, while the RMSE on depth was 0.11 m. The differences between the planimetric distances that were measured between the GCPs on the 3D model scaled using the georeferencing technique (by MBES) and those measured on the model scaled using the 3D trilateration technique were within 10 cm.

The major errors found in the X, Y (plan) were observed on the external points of the investigated area with respect to the central sector (Table 2) with centimetric accuracy, probably due to the lack of constraint points on the outermost sector. Similarly, the Z (depth) was also affected by the major error with decimetric accuracy (Table 3).

Table 2. Planimetric (X,Y) differences between LAS data corrected on MBES and LAS data corrected using the 3D trilateration method.

Target	LAS Corrected from MBES	LAS Corrected from 3D Trilateration	Difference X, Y
GCP1-GCP11	5.46 m	5.41 m	0.05 m
GCP1-GCP15	22.20 m	22.16 m	0.04 m
GCP11-GCP13	21.80 m	21.78 m	0.02 m
GCP1-GCP10	11.70 m	11.68 m	0.02 m
GCP10-GCP11	9.97 m	9.91 m	0.06 m
GCP10-GCP13	12.20 m	12.18 m	0.02 m
GCP10-GCP15	12.20 m	12.16 m	0.04 m
GCP13-GCP15	7.51 m	7,.48 m	0.03 m
GCP2-GCP13	12.10 m	12.18 m	−0.08 m
GCP2-GCP4	3.27 m	3.24 m	0.03 m
GCP4-GCP15	11.20 m	11.15 m	0.05 m
GCP13-GCP12	6.79 m	6.73 m	0.06 m
GCP15-GCP12	6.37 m	6.30 m	0.07 m
GCP2-GCP12	6.11 m	6.04 m	0.07 m
GCP4-GCP12	6.57 m	6.55 m	0.02 m

Table 3. Vertical Z (depth) difference between LAS data corrected on MBES and LAS data corrected using the 3D trilateration method.

Target	LAS Corrected on MBES	LAS Corrected from 3D Trilateration	Difference Z
GCP1	6.65 m	6.53 m	0.12 m
GCP2	7.40 m	7.53 m	−0.13 m
GCP3	6.46 m	6.30 m	0.16 m
GCP4	7.40 m	7.34 m	0.06 m
GCP6	7.10 m	7.01 m	0.09 m
GCP8	6.54 m	6.41 m	0.13 m
GCP9	7.09 m	6.98 m	0.11 m
GCP10	6.59 m	6.45 m	0.14 m
GCP11	6.49 m	6.33 m	0.16 m
GCP12	7.13 m	7.16 m	−0.02 m
GCP13	7.06 m	7.22 m	−0.16 m
GCP15	7.01 m	6.98 m	0.03 m

3.1. Object-Based Image Analysis (OBIA)

The Object-Based Image Analysis (OBIA) approach was used to obtain accurate thematic maps of the distribution of *P. oceanica* (Figure 13) and to define its boundaries to be processed in a GIS environment. The data acquired allowed us to compare the distribution of *P. oceanica* over two years and to verify its dynamic changes or stability in the initial area of restoration. Figure 13 shows the results of comparisons from surveys conducted at Cape Feto in October 2020 and August 2021. For the October 2020 orthomosaic, the most efficient object segmentation results, generated with Ecognition Essentials 10.2 software, were obtained on the basis of the following parameters: Scale = 250–1000; Color = 0.4; Smoothness = 0.4; Shape = 1; Compactness = 1. For the August 2021 orthomosaic, the best results for object segmentation were obtained using the following parameters: Scale = 150–400; Color = 0.6; Smoothness = 0.4; Shape = 1; Compactness = 1. For the October 2020 orthomosaic, an overall OBIA classification accuracy of 93.67% and a K-index value of 0.90 was obtained using the KNN algorithm (Table 4). Whereas, for the August 2021 orthomosaic, the overall accuracy was 99.02% the K-index value was 0.98 (Figure 13c and Table 4). Using OBIA classification of high-resolution orthomosaics, we estimated an increase in the extent of *P. oceanica* of approximately 7 m^2. Using the LIDAR classification tool of the Global Mapper software, we classified the point clouds of October 2020 and August 2021. The classification was performed using the shape of the OBIA classifications carried out for the two periods with the same thematic classes. The shape files were used to select the intersected points. An example of classification and comparison of the point clouds is shown in Figure 13. The results show that the LIDAR classification tool of the Global Mapper software is very efficient and practical for seagrass point cloud analysis.

Table 4. Accuracy of the classification of the restoration area of Capo Feto from the KNN machine learning algorithm for the orthomosaics of October 2020 and August 2021, respectively.

	(October 2020) Overall Accuracy: 93.67% K = 0.90		(August 2021) Overall Accuracy: 99.02% K = 0.98	
Thematic Classes	**User's Accuracy**	**Producer's Accuracy**	**User's Accuracy**	**Producer's Accuracy**
Dead matte	83.87%	100%	96.97%	100%
P. oceanica meadows	100%	86.67%	100%	100%
Rock	100%	95.65%	100%	95.45%

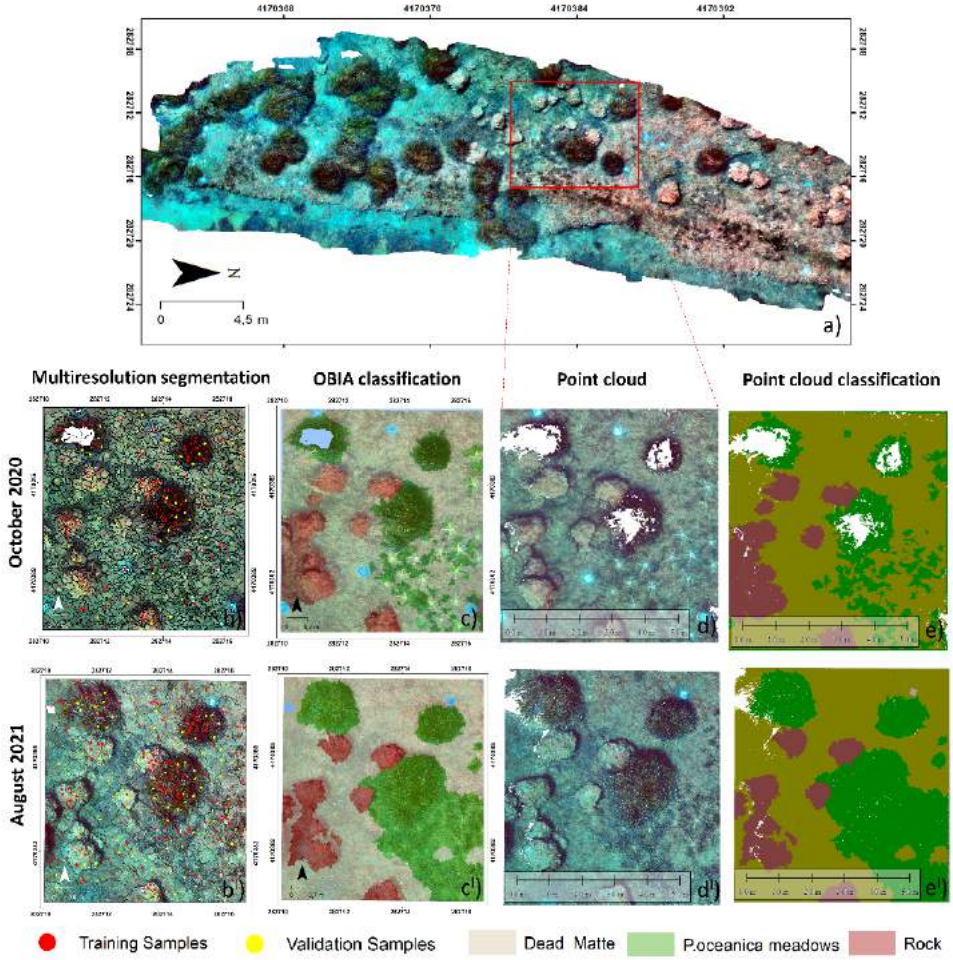

Figure 13. A comparison of the cloud point classification of the years 2020 and 2021 at the Capo Feto restoration site (Sicily) using the object segmentation technique. (**a**) Seafloor Orthomosaic map. (**b**,**b'**) Multiresolution segmentation, ground-truth training, and validation data. (**c**,**c'**) OBIA classification using the KNN algorithm. (**d**,**d'**) Point cloud data. (**e**,**e'**) Point cloud data classification.

3.2. Three-Dimensional Measurements and Analysis

To measure and analyze properly scaled and georeferenced dense point clouds, we used Cloud Compare software. We examined the height of the leaf canopy on four randomly selected *P. oceanica* patches identified in the area of interest shown in Figure 14. In total, the following height values were observed: 1.06 m for point 1, 0.91 m for point 2, 1.57 m for point 3, and finally 0.42 m for point 4 (Figure 14a). Moreover, elaborations were carried out with the tool "Extract Cloud Sections along polylines transect" to determine the height profiles of the leaf canopy for the entire LAS data point cloud (Figure 14b,c). The point clouds, in LAS data, represent a numerical model of the surface for which the elevation heights are reported, making it possible to measure the height of the leaf canopy and monitor its temporal change (Figure 14d).

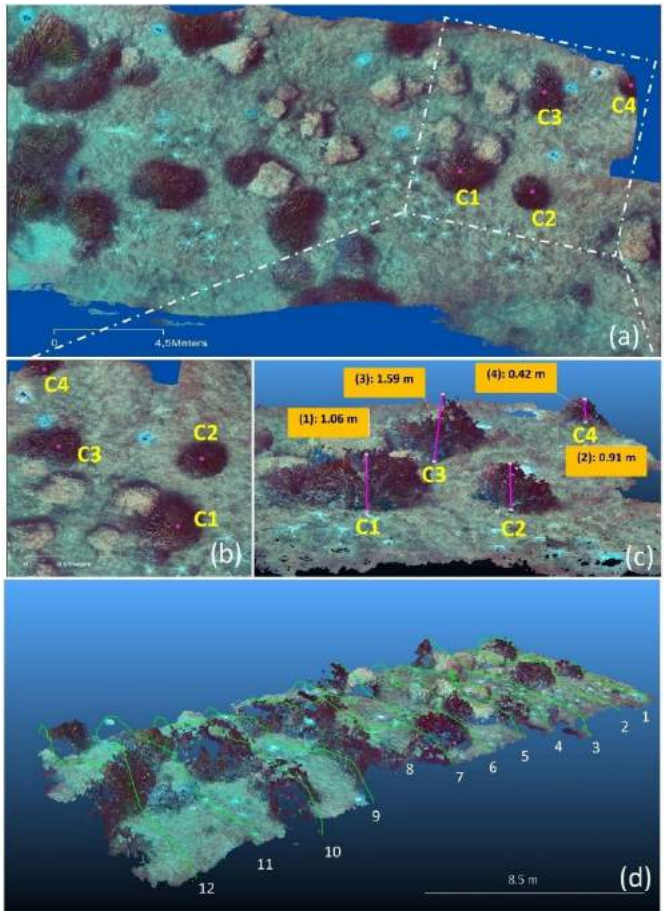

Figure 14. (**a**) Reconstruction of the dense point cloud of the Capo Feto site restoration. (**b**) an indication of areas measured in canopy heights. (**c**) a dense point cloud with identification of vertical height profiles. (**d**) leaf canopy profile measurement using Cloud Compare software.

4. Discussion

The successful application of seagrass restoration presupposes a thorough investigation of the site where the interventions are to be conducted. In the restoration areas, most of the environmental monitoring activities are conducted through direct observation by scuba divers, leading to mainly qualitative data [81].

Preliminary characterization of the sites should be conducted through traditional remote surveys by satellite images (panchromatic and multispectral), UAS surveys, and acoustic equipment (high-resolution multibeam and Side Scan Sonar data) for an extensive mapping of the seafloor of the study area [82]. However, underwater photogrammetry can be considered a very powerful tool for initially mapping seagrass transplants and then monitoring their progress for indications of the success of a restoration intervention. This is particularly so when assessing seagrass response in terms of growth and expansion of the canopy cover and height at a very high-resolution level.

Compared to the traditional monitoring of *P. oceanica* transplants, underwater photogrammetry provides high-resolution information from which microscale information can be extracted [22,23,34,83–88]. As highlighted in the literature, many restoration actions have failed, and this is often due to the erroneous choice of the intervention site and its characteristics, e.g., depth of the site and wave exposure, currents, and occurrence of boat anchoring [8]. It is therefore necessary to adopt a strict code of good practices for seagrass restoration interventions, which guides, step by step, accurate and careful management and monitoring of the entire process [8].

Therefore, the micro-bathymetry here proposed is the most appropriate tool to characterize both the donor and the receiving sites of the restoration actions [22,82]. Moreover,

the orthomosaic obtained from the DEM and the LAS dense point cloud are excellent tools for monitoring restoration sites, especially if used correctly during the identification and information collection phase. Underwater photogrammetry data (point clouds, DEMs, and orthomosaics), can reach subcentric resolutions higher than resolution multibeam data. In fact, the DEM produced by photogrammetry (Figure 15) allows the user to discriminate in detail not only the *P. oceanica* canopy and dead matte but also sandy areas and ripples, while the very high-resolution orthomosaic (Figure 15b) also shows the arrangement of dead leaves among the ripples.

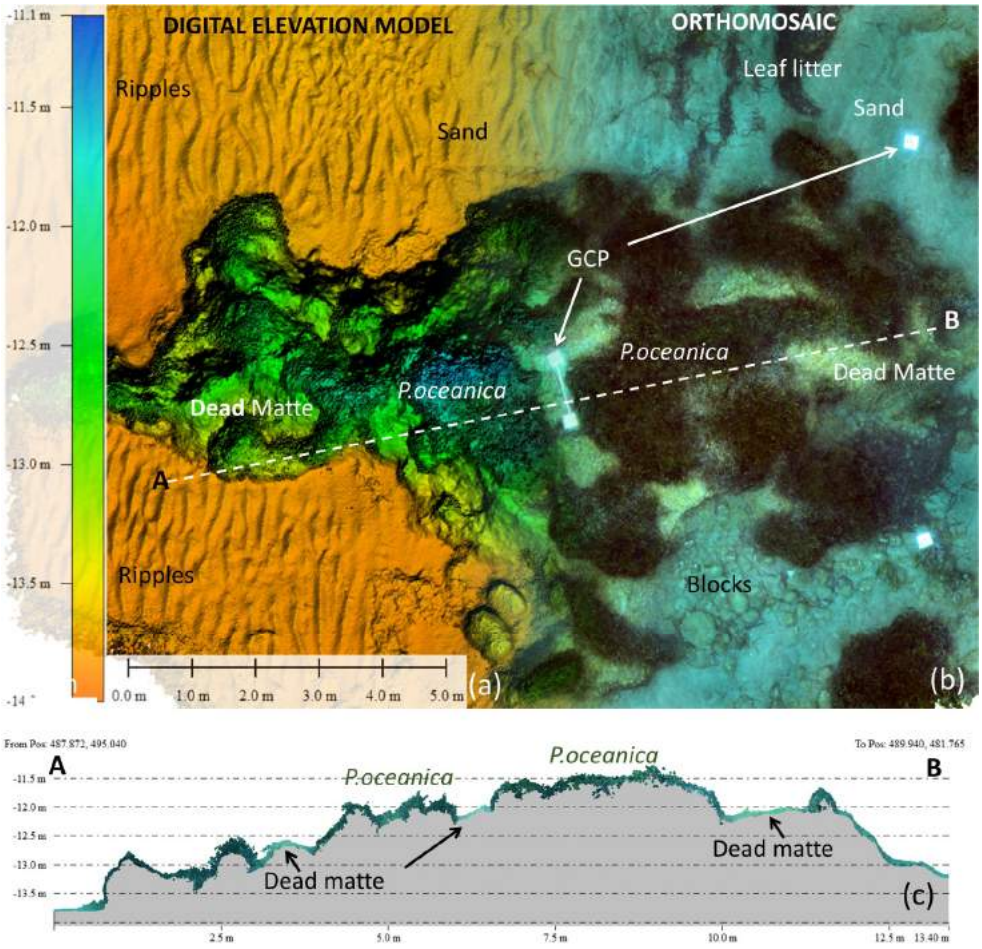

Figure 15. (**a**) Digital Elevation Model of *P. oceanica* meadows on matte at Ventotene Island. (**b**) Orthomosaic and DEM integration of *P. oceanica*. (**c**) AB bathymetric profile of leaf canopy height.

Compared to traditional methods for monitoring seagrass transplants, (e.g., measurement of plant biometry, shoot density, mortality rate, and growth rate of new cuttings), underwater photogrammetry complements and improves the above-mentioned surveillance and monitoring system, making it more informative and effective [7,89].

Restoration monitoring requires 3D metric and orthomosaic models that are accurately scaled and therefore it is necessary to adopt methodological procedures for correct and accurate environmental monitoring. First, it is necessary to calibrate the camera with which the images are acquired. Estimating the FOV of the camera is useful for defining the height at which the photogrammetric survey is to be carried out, for determining the number and length of the strips to be carried out, and finally the distance (overlap and sidelap) between the various strips.

During the acquisition of the images, it is necessary to guarantee the coverage of overlap and sidelap between all images. In a photogrammetric survey aiming at 3D reconstruction with Structure from Motion (SfM) techniques, it is important to guarantee a high

redundancy of the data, with some authors [87–89] suggesting that each zone of interest must be portrayed in at least nine photographs to guarantee an effective 3D reconstruction.

Greater accuracy in the use of underwater photogrammetry can be achieved by integrating photogrammetric data with very high-resolution information from multibeam bathymetry [14], which provides accurate georeferencing of the point cloud and the orthomosaic. This technique allows the accurate estimation of different descriptors, such as the surface, height, and volumes of the canopy [22], which are useful indicators of the success of seagrass restoration.

The use of high-resolution multibeam sounding to georeference the photogrammetric product data allows the use of very long transects over extensive areas (Figure 16) with accuracy employing ROVs, UAVs, and ASV systems. However, it should be remembered that multibeam data must be acquired on very high-frequency instruments (at least 400 kHz) and processed according to high-quality standards [14,32,87] (Figure 16).

The 3D trilateration technique represents a valid procedure for obtaining metric dense point clouds and orthomosaics without the need for multibeam bathymetry. As shown in this paper, the 3D trilateration conducted on eight control points represents a good trade-off between the work effort to be performed underwater and the obtainment of accurate data [90]. However, depending on the size of the area, more control points may be necessary to improve the reliability and accuracy of the resulting mapping products. Similarly, to improve the redundancy and control in the 3D trilateration technique, it is recommended to use the reinforced square protocols when extending the network [91].

The integration between the point cloud and high-resolution multibeam data, as evidenced by the RMSE values for the Capo Feto site, enables a more accurate planimetric/altimetric scaling of the dense point cloud since the multibeam surveys are carried out using differential correction positioning systems (RTK–PPK) and the Z-altitude values are corrected with the tidal data by local tide gauge stations.

Trilateration, as indicated in the Capo Feto survey, results in lower accuracy, especially at the altimetric level (RMSE 0.11). This is due to the lower precision and accuracy of the depth measurements obtained from the underwater dive computers, whose estimated error is approximately 10 cm [53].

The depths of the control points can be calculated by surveyors using a professional underwater pressure sensor, to be calibrated according to in situ temperature, salinity, and water density [49,53], and subsequently inserted in the processing phase of the photogrammetric data.

In trilateration, the measurement of distances between GCPs with the aid of a metric cable has limitations during underwater survey activities. So, to limit the diving time of the diving operators, it would be useful to have control bars with known measurements in the survey area, which can be used to measure distances between GCPs via software.

However, an effective solution for improving the accuracy of GCPs over large areas is to use a GNSS–RTK technique on permanent targets. These should be installed and used at mapping and monitoring sites to achieve multi-temporal detection of changes at the centimeter scale and on annual to decadal scales. [92,93].

Light conditions can compromise image quality and survey, depending on the depth of the survey and the presence of soot and turbidity [64]. In the presence of such problems, image enhancement algorithms (e.g., the ACE algorithm) can be a valuable tool for recovering image quality and improving the intelligibility of the orthomosaic and the LAS point cloud [31,94].

The classification of the orthomosaic, carried out using the Object-Based Image Analysis (OBIA) approach with the machine learning algorithm (KNN), represents a valid technique to extrapolate information on the coverage and distribution of the *P. oceanica* meadows subjected to restoration action and to estimate over time the increase in the area colonized.

Object-based classification (OBIA) using machine learning algorithms, as represented in [14,95], can properly extract the main features from orthomosaics or point cloud data.

Considering that the images can have GSD values between 0.3 cm/pixel and 2.2 cm/pixel, this information is useful to correctly determine the surface and the cover and to evaluate the expansion and regression rate of *P. oceanica* under restoration.

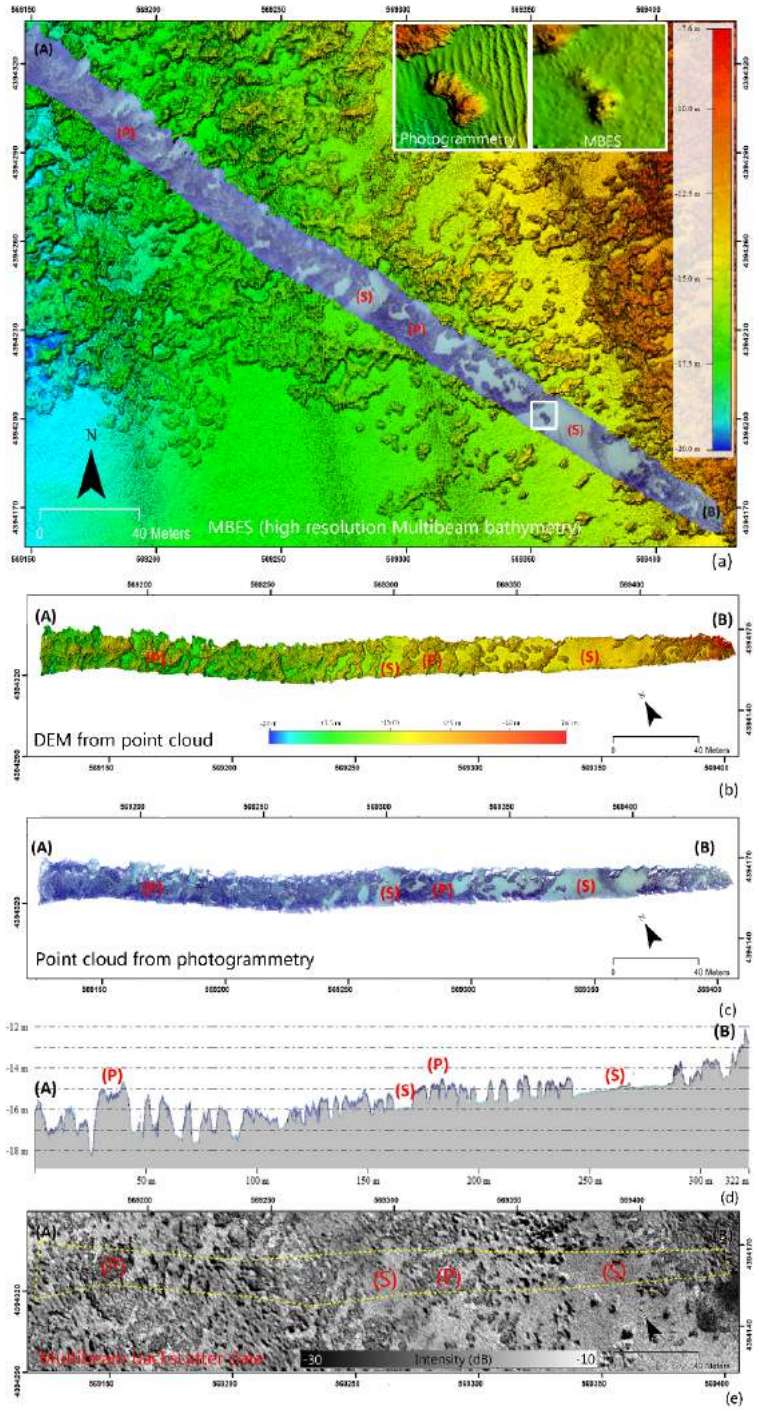

Figure 16. Bathymetric profile along the transect (AB) shows: (**a**) Co-registration of photogrammetric data from high-resolution (5 cm) multibeam bathymetry. (**b**) Very high-resolution DEM from point cloud. (**c**) RGB dense point cloud track line. (**d**) Bathymetric profile along the transect (AB) shows a comparison between the canopy height from photogrammetry and the DEM from high-resolution multibeam bathymetry. (**e**) Multibeam backscatter intensity map. The yellow dotted line indicates the area covered by the photogrammetric survey. (P: *P. oceanica*, S: sand).

The dense point cloud and the orthomosaics [88], obtained from the underwater photogrammetric survey, can also be used for computing ecological indices, such as the Conservation Index [96,97] and the Habitat Structure Index [98], to assess the conservation status of *P.oceanica* meadows.

Finally, the 3D analysis of the dense point cloud performed with the software Cloud Compare allows the determination of the height of the leaf canopy and the volume and evaluation of its growth over time. This parameter is therefore a new application approach that can be used in the future for estimating the trajectory of changes in transplanted meadows and associated stocks of carbon dioxide (CO_2) [99–101].

The height of the canopy makes it possible to evaluate the foliar biomass of *Posidonia oceanica,* from which it is possible to evaluate the annual capacity of carbon fixation and therefore of sequestration (it would be necessary to apply the inter-calibration in different sites where values of canopy height, biomass, and CO_2 fixation are available). This would make it possible to improve the assessment of the carbon fixation capacity of seagrass beds at many sites.

5. Conclusions

Traditional remote sensing technologies (MSI, MBES, and LIDAR) cannot provide ultra-fine-scale measurements of structural metrics such as seagrass distribution and abundance. They have either a very low spatial resolution or can be used only to map extensive areas in shallow waters.

To efficiently monitor the status of seagrass transplantation sites, ultra–very high-resolution and accurate mapping technologies must be adopted if the scope is to capture their microevolution in the short to long term. The high-resolution data that can be obtained through underwater photogrammetry, as demonstrated in this study, facilitate high-resolution data collection and offer a potential solution for improving field monitoring activities, including short- and long-term monitoring of *P. oceanica* meadow restoration activities at both the microscales and mesoscales.

Photogrammetric survey technologies offer tools to acquire and return information in accurate ways. The case studies here presented show the advantages of some techniques in obtaining the georeferencing of point clouds, DEMs, and orthomosaics and in the restitution of decimetric scale models. Compared to these advantages, however, one must consider the total time required for data processing, which depends on the resolution, quality, and number of images acquired. Photogrammetry requires a significant amount of computing power to generate high-resolution products for areas extending to several hundred square kilometers and is, therefore, practicable for limited areas.

Due to this limitation, along with other problems, such as reliable colour reproduction, only photogrammetric mapping of small marine areas is currently feasible. The use of Structure from Motion demonstrates the usefulness of this technology for expeditious surveys, on the one hand, because of the high accuracy of restitution, and, on the other hand, because it fits well into the context of multi-temporal monitoring of *P. oceanica* restoration sites.

The three-dimensional mapping procedures described, based on a combination of photogrammetry models and acoustic surveys, allow for accurate cartographic restitution in terms of ultra–high resolution and geospatial positioning and identification of objects and targets on the bottom.

To date, no remote sensing methodology has come close in terms of spatial resolution to the processing obtained through underwater photogrammetry. Additionally, this study technique for monitoring the seafloor and its benthic habitats can also be effectively used for other applied studies of marine geology and engineering for geo-hazard assessments and off-shore infrastructures.

Using the methodological approach described in this manuscript, it will be possible to accurately monitor seagrass restoration actions by contextualizing them in the three cartographic dimensions.

Therefore, we believe that habitat restoration interventions should be monitored and mapped with similar representations that irrefutably certify the intervention conducted so that anyone (scientists, technicians, etc.) can verify its presence, conservation status, and evolution, otherwise the efforts made so far to evaluate the success of global restoration actions could be in vain.

Author Contributions: Conceptualization, S.F.R., A.B. and A.T.; methodology, S.F.R., A.B., F.M. and A.L.; software, S.F.R., A.B., A.L. and U.S.; validation, S.C., A.T., F.B., G.P. and C.P.-M.; formal analysis, S.F.R., A.B., A.T. and A.L.; investigation, S.F.R., A.B., S.C., A.T. and V.R.; resources, S.C. and G.P.; data curation, S.F.R., A.B. and A.T.; writing—original draft preparation, S.F.R., A.B., A.T., A.D.I. and S.C.; writing—review and editing, S.F.R., A.B., A.T., F.M., A.L., A.D.I., M.M., S.C., G.P. and C.P.-M.; visualization, S.F.R. and A.B.; supervision, S.F.R., A.B., S.C., A.T. and F.B.; funding acquisition, S.F.R., S.C., A.T. and G.P. All authors have read and agreed to the published version of the manuscript.

Funding: This research has been conducted within Project PON_ARS01_00891, Conversion of Offshore Platforms for environmentally sustainable multiple uses—"PLACE" (CUP B66C18000380005), financed by MIUR funds and the European Union-Regional Development Fund. In Corsica, this research was funded by Foundation Setec, Office de l'Environnement de la Corse, and Office Français de la biodiversité as part of the RenforC project. This research has also been used for developing a methodology for the quantification of seagrass carbon sink in the SeaForest LIFE 17CCM/IT 000121 project.

Institutional Review Board Statement: Not applicable.

Informed Consent Statement: Not applicable.

Data Availability Statement: Not applicable.

Acknowledgments: The authors would like to thank the Nucleo Carabinieri Subacquei of Roma and Napoli for the photogrammetric survey conducted in Ventotene Island and Infraschi Bay.

Conflicts of Interest: The authors declare no conflict of interest.

References

1. Monnier, B.; Pergent, G.; Valette-Sansevin, A.; Boudouresque, C.F.; Mateo, M.A.; Pergent-Martini, C. The *Posidonia oceanica* matte: A unique coastal carbon sink for climate change mitigation and implications for management. *Vie et Milieu* **2020**, *70*, 17–24.
2. Costanza, R.; d'Arge, R.; de Groot, R.; Farber, S.; Grasso, M.; Hannon, B.; Limburg, K.; Naeem, S.; O'Neill, R.V.; Paruelo, J.; et al. The Value of the World's Ecosystem Services and Natural Capital. *Nature* **1997**, *387*, 253–260. [CrossRef]
3. Green, E.P.; Short, F.T. *World Atlas of Seagrasses*; University of California Press: Berkeley, CA, USA, 2003; ISBN 0-520-24047-2.
4. Waycott, M.; Duarte, C.M.; Carruthers, T.J.B.; Orth, R.J.; Dennison, W.C.; Olyarnik, S.; Calladine, A.; Fourqurean, J.W.; Heck, K.L.; Hughes, A.R.; et al. Accelerating Loss of Seagrasses across the Globe Threatens Coastal Ecosystems. *Proc. Natl. Acad. Sci. USA* **2009**, *106*, 12377–12381. [CrossRef]
5. Cullen-Unsworth, L.C.; Unsworth, R. A call for seagrass protection. *Science* **2018**, *361*, 446–448. [CrossRef] [PubMed]
6. Katwijk, M.M.; Thorhaug, A.; Marbà, N.; Orth, R.J.; Duarte, C.M.; Kendrick, G.A.; Althuizen, I.H.J.; Balestri, E.; Bernard, G.; Cambridge, M.L.; et al. Global Analysis of Seagrass Restoration: The Importance of Large-scale Planting. *J. Appl. Ecol.* **2016**, *53*, 567–578. [CrossRef]
7. Calvo, S.; Calvo, R.; Luzzu, F.; Raimondi, V.; Assenzo, M.; Cassetti, F.; Tomasello, A. Performance Assessment of *Posidonia oceanica* (L.) Delile Restoration Experiment on Dead Matte Twelve Years after Planting—Structural and Functional Meadow Features. *Water* **2021**, *13*, 724. [CrossRef]
8. Boudouresque, C.-F.; Blanfuné, A.; Pergent, G.; Thibaut, T. Restoration of Seagrass Meadows in the Mediterranean Sea: A Critical Review of Effectiveness and Ethical Issues. *Water* **2021**, *13*, 1034. [CrossRef]
9. Di Maida, G.; Tomasello, A.; Luzzu, F.; Scannavino, A.; Pirrotta, M.; Orestano, C.; Calvo, S. Discriminating between *Posidonia oceanica* Meadows and Sand Substratum Using Multibeam Sonar. *ICES J. Mar. Sci.* **2011**, *68*, 12–19. [CrossRef]
10. Lo Iacono, C.; Mateo, M.A.; Gràcia, E.; Guasch, L.; Carbonell, R.; Serrano, L.; Serrano, O.; Dañobeitia, J. Very High-Resolution Seismo-Acoustic Imaging of Seagrass Meadows (Mediterranean Sea): Implications for Carbon Sink Estimates. *Geophys. Res. Lett.* **2008**, *35*, 18. [CrossRef]
11. Veettil, B.K.; Ward, R.D.; Lima, M.D.A.C.; Stankovic, M.; Hoai, P.N.; Quang, N.X. Opportunities for Seagrass Research Derived from Remote Sensing: A Review of Current Methods. *Ecol. Indic.* **2020**, *117*, 106560. [CrossRef]
12. Pasqualini, V.; Clabaut, P.; Pergent, G.; Benyoussef, L.; Pergent-Martini, C. Contribution of Side Scan Sonar to the Management of Mediterranean Littoral Ecosystems. *Int. J. Remote Sens.* **2000**, *21*, 367–378. [CrossRef]

13. Pergent, G.; Monnier, B.; Clabaut, P.; Gascon, G.; Pergent-Martini, C.; Valette-Sansevin, A. Innovative Method for Optimizing Side-Scan Sonar Mapping: The Blind Band Unveiled. *Estuar. Coast. Shelf Sci.* **2017**, *194*, 77–83. [CrossRef]
14. Rende, S.F.; Bosman, A.; Di Mento, R.; Bruno, F.; Lagudi, A.; Irving, A.D.; Dattola, L.; Giambattista, L.D.; Lanera, P.; Proietti, R.; et al. Ultra-High-Resolution Mapping of *Posidonia oceanica* (L.) Delile Meadows through Acoustic, Optical Data and Object-Based Image Classification. *J. Mar. Sci. Eng.* **2020**, *8*, 647. [CrossRef]
15. Rende, F.S.; Irving, A.D.; Lagudi, A.; Bruno, F.; Scalise, S.; Cappa, P.; Montefalcone, M.; Bacci, T.; Penna, M.; Trabucco, B.; et al. Pilot application of 3D underwater imaging techniques for mapping *Posidonia oceanica* (L.) Delile meadows. *Int. Arch. Photogramm. Remote Sens. Spat. Inf. Sci.* **2015**, *40*, 177–181. [CrossRef]
16. Ventura, D.; Bonifazi, A.; Gravina, M.F.; Belluscio, A.; Ardizzone, G. Mapping and Classification of Ecologically Sensitive Marine Habitats Using Unmanned Aerial Vehicle (UAV) Imagery and Object-Based Image Analysis (OBIA). *Remote Sens.* **2018**, *10*, 1331. [CrossRef]
17. Tomasello, A.; Cassetti, F.P.; Savona, A.; Pampalone, V.; Pirrotta, M.; Calvo, S.; Signa, G.; Andolina, C.; Mazzola, A.; Vizzini, S.; et al. The use of very high resolution images for studying *Posidonia oceanica* reefs. *Vie et Milieu* **2020**, *70*, 25–35.
18. Bryson, M.; Ferrari, R.; Figueira, W.; Pizarro, O.; Madin, J.; Williams, S.; Byrne, M. Characterization of Measurement Errors Using Structure-from-Motion and Photogrammetry to Measure Marine Habitat Structural Complexity. *Ecol. Evol.* **2017**, *7*, 5669–5681. [CrossRef]
19. Nocerino, E.; Menna, F.; Gruen, A.; Troyer, M.; Capra, A.; Castagnetti, C.; Rossi, P.; Brooks, A.J.; Schmitt, R.J.; Holbrook, S.J. Coral Reef Monitoring by Scuba Divers Using Underwater Photogrammetry and Geodetic Surveying. *Remote Sens.* **2020**, *12*, 3036. [CrossRef]
20. Piazza, P.; Cummings, V.; Guzzi, A.; Hawes, I.; Lohrer, D.; Marini, S.; Marriott, P.; Menna, F.; Nocerino, E.; Peirano, A.; et al. Underwater photogrammetry in Antarctica: Long-term observations in benthic ecosystems and legacy data rescue. *Polar Biol.* **2019**, *42*, 1061–1079. [CrossRef]
21. Piazza, P.; Cummings, V.J.; Lohrer, D.M.; Marini, S.; Marriott, P.; Menna, F.; Nocerino, E.; Peirano, A.; Schiapa-relli, S. Divers-operated underwater photogrammetry: Applications in the study of antarctic benthos. *Int. Arch. Photogramm. Remote Sens. Spat. Inf. Sci.* **2018**, *42*, 885–892. [CrossRef]
22. Rende, S.F.; Irving, A.D.; Bacci, T.; Parlagreco, L.; Bruno, F.; De Filippo, F.; Montefalcone, M.; Penna, M.; Trabucco, B.; Di Mento, R.; et al. Advances in Micro-Cartography: A Two-Dimensional Photo Mosaicing Technique for Seagrass Monitoring. *Estuar. Coast. Shelf Sci.* **2015**, *167*, 475–486. [CrossRef]
23. Marre, G.; Holon, F.; Luque, S.; Boissery, P.; Deter, J. Monitoring Marine Habitats With Photogrammetry: A Cost-Effective, Accurate, Precise and High-Resolution Reconstruction Method. *Front. Mar. Sci.* **2019**, *6*, 1–15. [CrossRef]
24. Marre, G.; Deter, J.; Holon, F.; Boissery, P.; Luque, S. Fine-Scale Automatic Mapping of Living *Posidonia oceanica* Seagrass Beds with Underwater Photogrammetry. *Mar. Ecol. Prog. Ser.* **2020**, *643*, 63–74. [CrossRef]
25. Pasqualini, V.; Pergent-Martini, C.; Clabaut, P.; Marteel, H.; Pergent, G. Integration of aerial remote sensing, photogrammetry, and GIS technologies in seagrass mapping. *Photogramm. Eng. Remote Sens.* **2001**, *67*, 99–105.
26. Mizuno, K.; Asada, A.; Matsumoto, Y.; Sugimoto, K.; Fujii, T.; Yamamuro, M.; Fortes, M.D.; Sarceda, M.; Jimenez, L.A. A Simple and Efficient Method for Making a High-Resolution Seagrass Map and Quantification of Dugong Feeding Trail Distribution: A Field Test at Mayo Bay, Philippines. *Ecol. Inform.* **2017**, *38*, 89–94. [CrossRef]
27. Casella, E.; Collin, A.; Harris, D.; Ferse, S.; Bejarano, S.; Parravicini, V.; Hench, J.L.; Rovere, A. Mapping Coral Reefs Using Consumer-Grade Drones and Structure from Motion Photogrammetry Techniques. *Coral Reefs* **2017**, *36*, 269–275. [CrossRef]
28. Ventura, D.; Mancini, G.; Casoli, E.; Pace, D.S.; Lasinio, G.J.; Belluscio, A.; Ardizzone, G. Seagrass Restoration Monitoring and Shallow-Water Benthic Habitat Mapping through a Photogrammetry-Based Protocol. *J. Environ. Manag.* **2022**, *304*, 114262. [CrossRef]
29. Shortis, M. Camera Calibration Techniques for Accurate Measurement Underwater. In *3D Recording and Interpretation for Maritime Archaeology*; Coastal Research Library; McCarthy, J.K., Benjamin, J., Winton, T., van Duivenvoorde, W., Eds.; Springer International Publishing: Cham, Switzerland, 2019; Volume 31, pp. 11–27. ISBN 978-3-030-03634-8.
30. Menna, F.; Nocerino, E.; Fassi, F.; Remondino, F. Geometric and optic characterization of a hemispherical dome port for underwater photogrammetry. *Sensors* **2016**, *16*, 48. [CrossRef]
31. Mangeruga, M.; Cozza, M.; Bruno, F. Evaluation of Underwater Image Enhancement Algorithms under Different Environmental Conditions. *J. Mar. Sci. Eng.* **2018**, *6*, 10. [CrossRef]
32. Kwasnitschka, T.; Köser, K.; Sticklus, J.; Rothenbeck, M.; Weiß, T.; Wenzlaff, E.; Schoening, T.; Triebe, L.; Steinführer, A.; Devey, C.; et al. DeepSurveyCam—A Deep Ocean Optical Mapping System. *Sensors* **2016**, *16*, 164. [CrossRef]
33. Johnson-Roberson, M.; Bryson, M.; Friedman, A.; Pizarro, O.; Troni, G.; Ozog, P.; Henderson, J.C. High-Resolution Underwater Robotic Vision-Based Mapping and Three-Dimensional Reconstruction for Archaeology. *J. Field Robot.* **2017**, *34*, 625–643. [CrossRef]
34. Bonin-Font, F.; Campos, M.M.; Codina, G.O. Towards Visual Detection, Mapping and Quantification of *Posidonia oceanica* Using a Lightweight AUV. *IFAC-PapersOnLine* **2016**, *49*, 500–505. [CrossRef]
35. Drap, P.; Seinturier, J.; Conte, G.; Caiti, A.; Scaradozzi, D.; Zanoli, S.M.; Gambogi, P. Underwater cartography for archaeology in the VENUS project. *Geomatica* **2008**, *62*, 419–427.

36. Drap, P.; Seinturier, J.; Hijazi, B.; Merad, D.; Boi, J.-M.; Chemisky, B.; Seguin, E.; Long, L. The ROV 3D Project: Deep-Sea Underwater Survey Using Photogrammetry: Applications for Underwater Archaeology. *J. Comput. Cult. Herit.* **2015**, *8*, 1–24. [CrossRef]
37. Menna, F.; Nocerino, E.; Nawaf, M.; Seinturier, J.; Torresani, A.; Drap, P.; Remondino, F.; Chemisky, B. Towards Real-Time Underwater Photogrammetry for Subsea Metrology Applications. In Proceedings of the OCEANS 2019—Marseille, Marseille, France, 17–20 June 2019; pp. 1–10. [CrossRef]
38. Balletti, C.; Beltrame, C.; Costa, E.; Guerra, F.; Vernier, P. Underwater photogrammetry and 3D reconstruction of marble cargos shipwreck. *Int. Arch. Photogramm. Remote Sens. Spat. Inf. Sci.* **2015**, *XL-5-W5*, 7–13. [CrossRef]
39. Bass, G.F. *Archaeology Under Water*; Thames & Hudson and Praeger: London, UK; New York, NY, USA, 1966.
40. Green, J.N. *Maritime Archaeology: A Technical Handbook*, 2nd ed.; Routledge: London, UK; New York, NY, USA, 2020; ISBN 978-0-367-60560-5.
41. Bojakowski, P.; Bojakowski, K.C.; Naughton, P. A Comparison Between Structure from Motion and Direct Survey Methodologies on the Warwick. *J. Marit. Archaeol.* **2015**, *10*, 159–180. [CrossRef]
42. Skarlatos, D.; Menna, F.; Nocerino, E.; Agrafiotis, P. Precision potential of underwater networks for archaeological excavation through trilateration and photogrammetry. *Int. Arch. Photogramm. Remote Sens. Spat. Inf. Sci.* **2019**, *42*, 175–180. [CrossRef]
43. Calantropio, A.; Chiabrando, F.; Auriemma, R. Photogrammetric underwater and UAS surveys of archaeological sites: The case study of the roman shipwreck of Torre Santa Sabina. *Int. Arch. Photogramm. Remote Sens. Spat. Inf. Sci.* **2021**, *XLIII-B2-2021*, 643–650. [CrossRef]
44. Chemisky, B.; Menna, F.; Nocerino, E.; Drap, P. Underwater Survey for Oil and Gas Industry: A Review of Close Range Optical Methods. *Remote Sens.* **2021**, *13*, 2789. [CrossRef]
45. Menna, F.; Agrafiotis, P.; Georgopoulos, A. State of the Art and Applications in Archaeological Underwater 3D Recording and Mapping. *J. Cult. Herit.* **2018**, *33*, 231–248. [CrossRef]
46. Massot-Campos, M.; Oliver-Codina, G. Optical Sensors and Methods for Underwater 3D Reconstruction. *Sensors* **2015**, *15*, 9864. [CrossRef] [PubMed]
47. Shortis, M.R.; Ravanbakskh, M.; Shaifat, F.; Harvey, E.S.; Mian, A.; Seager, J.W.; Culverhouse, P.F.; Cline, D.E.; Edgington, D.R. A Review of Techniques for the Identification and Measurement of Fish in Underwater Stereo-Video Image Sequences. In *Proceedings of the Videometrics, Range Imaging, and Applications XII; and Automated Visual Inspection*; SPIE: Munich, Germany, 2013; Volume 8791, pp. 107–116.
48. Istenič, K.; Gracias, N.; Arnaubec, A.; Escartín, J.; Garcia, R. Automatic Scale Estimation of Structure from Motion Based 3D Models Using Laser Scalers in Underwater Scenarios. *ISPRS J. Photogramm. Remote Sens.* **2020**, *159*, 13–25. [CrossRef]
49. Menna, F.; Nocerino, E.; Chemisky, B.; Remondino, F.; Drap, P. Accurate scaling and levelling in underwater photogrammetry with a pressure sensor. *Int. Arch. Photogramm. Remote Sens. Spat. Inf. Sci.* **2021**, *XLIII-B2-2021*, 667–672. [CrossRef]
50. Rule, N. The Direct Survey Method (DSM) of Underwater Survey, and Its Application Underwater. *Int. J. Naut. Archaeol.* **1989**, *18*, 157–162. [CrossRef]
51. Costa, E. The progress of survey techniques in underwater sites: The case study of Cape Stoba shipwreck. *Int. Arch. Photogramm. Remote Sens. Spat. Inf. Sci.* **2019**, *42*, 69–75. [CrossRef]
52. Neyer, F.; Nocerino, E.; Gruen, A. Monitoring Coral Growth—The Dichotomy Between Underwater Photogrammetry and Geodetic Control Network. *Int. Arch. Photogramm. Remote Sens. Spat. Inf. Sci.* **2018**, *422*, 759–766. [CrossRef]
53. Azzopardi, E.; Sayer, M. Estimation of Depth and Temperature in 47 Models of Diving Decompression Computer. *Underw. Technol.* **2012**, *31*, 3–12. [CrossRef]
54. Cramer, M.; Stallmann, D.; Haala, N. Direct georeferencing using GPS/inertial exterior orientations for photogrammetric applications. *Int. Arch. Photogramm. Remote Sens.* **2000**, *33*, 198–205.
55. Abadie, A.; Boissery, P.; Viala, C. Georeferenced Underwater Photogrammetry to Map Marine Habitats and Submerged Artificial Structures. *Photogramm. Rec.* **2018**, *33*, 448–469. [CrossRef]
56. Bruno, F.; Lagudi, A.; Passaro, S.; Saggoimo, R. Opto-acoustic 3D reconstruction of the "Punta Scifo D" shipwreck. In *1st IMEKO TC4 International Workshop on Metrology for Geotechnics*; MetroGeotechnics: Benevento, Italy, 2016; pp. 327–333.
57. Hossain, M.D.; Chen, D. Segmentation for Object-Based Image Analysis (OBIA): A Review of Algorithms and Challenges from Remote Sensing Perspective. *ISPRS J. Photogramm. Remote Sens.* **2019**, *150*, 115–134. [CrossRef]
58. Roelfsema, C.M.; Lyons, M.; Kovacs, E.M.; Maxwell, P.; Saunders, M.I.; Samper-Villarreal, J.; Phinn, S.R. Multi-Temporal Mapping of Seagrass Cover, Species and Biomass: A Semi-Automated Object Based Image Analysis Approach. *Remote Sens. Environ.* **2014**, *150*, 172–187. [CrossRef]
59. Badenko, V.; Zotov, D.; Muromtseva, N.; Volkova, Y.; Chernov, P. Comparison of software for airborne laser scanning data processing in smart city applications. *Int. Arch. Photogramm. Remote Sens. Spat. Inf. Sci.* **2019**, *XLII-5-W2*, 9–13. [CrossRef]
60. Pirrotta, M.; Tomasello, A.; Scannavino, A.; Maida, G.D.; Luzzu, F.; Bellissimo, G.; Bellavia, C.; Costantini, C.; Orestano, C.; Sclafani, G.; et al. Transplantation Assessment of Degraded *Posidonia oceanica* Habitats: Site Selection and Long-Term Monitoring. *Mediterr. Mar. Sci.* **2015**, *16*, 591–604. [CrossRef]
61. Lester, S.E.; Dubel, A.K.; Hernán, G.; McHenry, J.; Rassweiler, A. Spatial Planning Principles for Marine Ecosystem Restoration. *Front. Mar. Sci.* **2020**, *7*, 328. [CrossRef]

62. Short, F.; Davis, R.; Kopp, B.; Short, C.; Burdick, D. Site-Selection Model for Optimal Transplantation of Eelgrass Zostera Marina in the Northeastern US. *Mar. Ecol. Prog. Ser.* **2002**, *227*, 253–267. [CrossRef]
63. Calvo, S.; Pirrotta, M.; Tomasello, A. Letter to the editor regarding the article "*Taking advantage of seagrass recovery potential to develop novel and effective meadow rehabilitation methods*" by Alagna et al., published in Marine Pollution Bulletin, 149: 2019 (110578). *Mar. Pollut. Bull.* **2020**, *158*, 111395. [CrossRef]
64. Brown, D.C. Close-Range Camera Calibration. *Photogramm. Eng.* **1971**, *37*, 855–866.
65. Menna, F.; Nocerino, E.; Remondino, F. Flat versus hemispherical dome ports in underwater photogrammetry. *Int. Arch. Photogramm. Remote Sens. Spat. Inf. Sci.* **2017**, *42*, 481. [CrossRef]
66. Nocerino, E.; Menna, F.; Remondino, F. Accuracy of typical photogrammetric networks in cultural heritage 3D modeling projects. *Int. Arch. Photogramm. Remote Sens. Spat. Inf. Sci.* **2014**, *40*, 465. [CrossRef]
67. Shortis, M. Calibration techniques for accurate measurements by underwater camera systems. *Sensors* **2015**, *15*, 9831. [CrossRef]
68. Helmholz, P.; Long, J.; Munsie, T.; Belton, D. Accuracy assessment of GOPROHero 3 (black) camera in underwater environment. *Int. Arch. Photogramm. Remote Sens. Spat. Inf. Sci.* **2016**, *41*, 477–483. [CrossRef]
69. Nocerino, E.; Menna, F.; Farella, E.; Remondino, F. 3D virtualization of an underground semi-submerged cave system. *Int. Arch. Photogramm. Remote Sens. Spat.-Form. Sci.* **2019**, *XLII-2/W15*, 857–864. [CrossRef]
70. Nocerino, E.; Nawaf, M.M.; Saccone, M.; Ellefi, M.B.; Pasquet, J.; Royer, J.P.; Drap, P. Multi-camera system calibration of a low-cost remotely operated vehicle for underwater cave exploration. *Int. Arch. Photogramm. Remote Sens. Spat. Inf. Sci.* **2018**, *42*, 329–337. [CrossRef]
71. Nocerino, E.; Neyer, F.; Grün, A.; Troyer, M.; Menna, F.; Brooks, A.; Capra, A.; Castagnetti, C.; Rossi, P. Comparison of diver-operated underwater photogrammetric systems for coral reef monitoring. *ISPRS-Int. Arch. Photogramm. Remote Sens. Spat. Inf. Sci.* **2019**, *42*, 143–150. [CrossRef]
72. AgisoftMetashape. Available online: https://www.agisoft.com/ (accessed on 16 July 2021).
73. Bosman, A.; Casalbore, D.; Anzidei, M.; Carmisciano, C.; Chiocci, F. The first ultra-high resolution digital terrain model of the shallow-water sector around Lipari Island (Aeolian Islands, Italy). *Ann. Geophys.* **2015**, *58*, 5. [CrossRef]
74. Bosman, A.; Romagnoli, C.; Madricardo, F.; Correggiari, A.; Remia, A.; Zubalich, R.; Fogarin, S.; Kruss, A.; Trincardi, F. Short-Term Evolution of Po Della Pila Delta Lobe from Time Lapse High-Resolution Multibeam Bathymetry (2013–2016). *Estuar. Coast. Shelf Sci.* **2020**, *233*, 106533. [CrossRef]
75. Image Enhancement Process Tool. Available online: https://imareculture.eu/downloads/project-tools/image-enhancement-process-tool/ (accessed on 16 July 2021).
76. Getreuer, P. Automatic Color Enhancement (ACE) and Its Fast Implementation. *Image Process. Line* **2012**, *2*, 266–277. [CrossRef]
77. Global Mapper. Available online: https://www.bluemarblegeo.com/global-mapper/ (accessed on 16 July 2021).
78. Site Recorder 4. Available online: http://www.3hconsulting.com/ProductsRecorderMain.html (accessed on 16 July 2021).
79. Trimble eCognition Essentil. Available online: https://geospatial.trimble.com/products-and-solutions/ecognition-essentials (accessed on 16 July 2021).
80. Cloud Compare. Available online: http://cloudcompare.org/ (accessed on 16 July 2021).
81. Van Katwijk, M.M.; Bos, A.R.; de Jonge, V.N.; Hanssen, L.S.A.M.; Hermus, D.C.R.; de Jong, D.J. Guidelines for Seagrass Restoration: Importance of Habitat Selection and Donor Population, Spreading of Risks, and Ecosystem Engineering Effects. *Mar. Pollut. Bull.* **2009**, *58*, 179–188. [CrossRef]
82. Gumusay, M.U.; Bakirman, T.; TuneyKizilkaya, I.; Aykut, N.O. A Review of Seagrass Detection, Mapping and Monitoring Applications Using Acoustic Systems. *Eur. J. Remote Sens.* **2019**, *52*, 1–29. [CrossRef]
83. Hu, W.; Zhang, D.; Chen, B.; Liu, X.; Ye, X.; Jiang, Q.; Zheng, X.; Du, J.; Chen, S. Mapping the Seagrass Conservation and Restoration Priorities: Coupling Habitat Suitability and Anthropogenic Pressures. *Ecol. Indic.* **2021**, *129*, 107960. [CrossRef]
84. Uhrin, A.V.; Kirsch, K. Prioritizing seagrass restoration sites: Study examines predictors of seagrass bed recovery. In *GIS for the Oceans*; ESRI: Redlands, CA, USA, 2011; pp. 49–54.
85. Klemas, V. Using Remote Sensing to Select and Monitor Wetland Restoration Sites: An Overview. *J. Coast. Res.* **2013**, *289*, 958–970. [CrossRef]
86. Ridge, J.T.; Johnston, D.W. Unoccupied Aircraft Systems (UAS) for Marine Ecosystem Restoration. *Front. Mar. Sci.* **2020**, *7*, 438. [CrossRef]
87. Figueira, W.; Ferrari, R.; Weatherby, E.; Porter, A.; Hawes, S.; Byrne, M. Accuracy and Precision of Habitat Structural Complexity Metrics Derived from Underwater Photogrammetry. *Remote Sens.* **2015**, *7*, 5859. [CrossRef]
88. Hatcher, G.A.; Warrick, J.A.; Ritchie, A.C.; Dailey, E.T.; Zawada, D.G.; Kranenburg, C.; Yates, K.K. Accurate Bathymetric Maps From Underwater Digital Imagery Without Ground Control. *Front. Mar. Sci.* **2020**, *7*, 525. [CrossRef]
89. Tan, Y.M.; Dalby, O.; Kendrick, G.A.; Statton, J.; Sinclair, E.A.; Fraser, M.W.; Macreadie, P.I.; Gillies, C.L.; Coleman, R.A.; Waycott, M.; et al. Seagrass Restoration Is Possible: Insights and Lessons From Australia and New Zealand. *Front. Mar. Sci.* **2020**, *7*, 617. [CrossRef]
90. Bianco, S.; Ciocca, G.; Marelli, D. Evaluating the Performance of Structure from Motion Pipelines. *J. Imaging* **2018**, *4*, 98. [CrossRef]
91. Moniruzzaman, M.; Islam, S.M.S.; Lavery, P.; Bennamoun, M.; Lam, C.P. Imaging and Classification Techniques for Seagrass Mapping and Monitoring: A Comprehensive Survey. *arXiv* **2019**, arXiv:1902.11114.

92. Rossi, P.; Castagnetti, C.; Capra, A.; Brooks, A.J.; Mancini, F. Detecting Change in Coral Reef 3D Structure Using Underwater Photogrammetry: Critical Issues and Performance Metrics. *Appl. Geomat.* **2020**, *12*, 3–17. [CrossRef]
93. Chemisky, B.; Nocerino, E.; Menna, F.; Nawaf, M.M.; Drap, P. A portable opto-acoustic survey solution for mapping of underwater targets. *Int. Arch. Photogramm. Remote Sens. Spat. Inf. Sci.* **2021**, *XLIII-B2-2021*, 651–658. [CrossRef]
94. Gatta, C.; Rizzi, A.; Marini, D. ACE: An automatic color equalization algorithm. In Proceedings of the First European Conference on Color in Graphics Image and Vision (CGIV02), University of Poitiers, Poitiers, France, 2–4 April 2002.
95. Lathrop, R.G.; Montesano, P.; Haag, S. A Multi-Scale Segmentation Approach to Mapping Seagrass Habitats Using Airborne Digital Camera Imagery. *Photogramm. Eng. Remote Sens.* **2006**, *72*, 665–675. [CrossRef]
96. Moreno, D.; Aguilera, P.; Castro, H. Assessment of the Conservation Status of Seagrass (*Posidonia oceanica*) Meadows: Implications for Monitoring Strategy and the Decision-Making Process. *Biol. Conserv.* **2001**, *102*, 325–332. [CrossRef]
97. Montefalcone, M. Ecosystem Health Assessment Using the Mediterranean Seagrass *Posidonia oceanica*: A Review. *Ecol. Indic.* **2009**, *9*, 595–604. [CrossRef]
98. Irving, A.D.; Tanner, J.E.; Gaylard, S.G. An Integrative Method for the Evaluation, Monitoring, and Comparison of Seagrass Habitat Structure. *Mar. Pollut. Bull.* **2013**, *66*, 176–184. [CrossRef]
99. Greiner, J.T.; McGlathery, K.J.; Gunnell, J.; McKee, B.A. Seagrass Restoration Enhances "Blue Carbon" Sequestration in Coastal Waters. *PLoS ONE* **2013**, *8*, e72469. [CrossRef]
100. Thorhaug, A.; Poulos, H.M.; López-Portillo, J.; Ku, T.C.W.; Berlyn, G.P. Seagrass Blue Carbon Dynamics in the Gulf of Mexico: Stocks, Losses from Anthropogenic Disturbance, and Gains through Seagrass Restoration. *Sci. Total Environ.* **2017**, *605–606*, 626–636. [CrossRef]
101. Pergent-Martini, C.; Pergent, G.; Monnier, B.; Boudouresque, C.-F.; Mori, C.; Valette-Sansevin, A. Contribution of *Posidonia oceanica* meadows in the context of climate change mitigation in the Mediterranean Sea. *Mar. Environ. Res.* **2021**, *165*, 105236. [CrossRef]